DEUTSCHES ELEKTRONEN-SYNCHROTRON DESY

DESY 83-007
February 1983

QCD AND HADRON JETS -- NEW RESULTS FROM PEP AND PETRA

by

Sau Lan Wu

Department of Physics, University of Wisconsin, Madison, Wisconsin

and

Deutsches Elektronen-Synchrotron DESY, Hamburg

ISSN 0418-9833

NOTKESTRASSE 85 · 2 HAMBURG 52

To be sure that your preprints are promptly included in the HIGH ENERGY PHYSICS INDEX , send them to the following address (if possible by air mail) :

DESY
Bibliothek
Notkestrasse 85
2 Hamburg 52
Germany

DESY 83-007
February 1983

ISSN 0418-9833

QCD AND HADRON JETS -- NEW RESULTS FROM PEP AND PETRA *

by

Sau Lan Wu

Department of Physics, University of Wisconsin, Madison, Wisconsin, USA†

and

Deutsches Elektronen-Synchrotron DESY, Hamburg, Germany

Abstract

Recent experimental data related to hadron jets and QCD are reviewed from the ten detectors at PEP and PETRA. The many interesting new results include the measurements of the quark-gluon coupling constant α_s, the total hadronic cross section, and the gluon spin with high statistics, a possible difference between the quark and gluon jets, particle identification in jets, and a search for charged Higgs and technipions from four-jet events. The fragmentation functions for the heavy quarks (charm and bottom) are discussed in this Conference by Schlatter of SLAC.

* Rapporteur talk at the Topical Conference of the 1982 SLAC Summer Institute on Particle Physics, August 16 - 27, 1982, SLAC, Stanford, California, USA.

† Supported by the US Department of Energy Contract EY-76-C-02-0881.

1. INTRODUCTION

The most important problems of particle physics can be stated as the "gauge problem" and the "mass problem". Gauge theory describes successfully both the strong interactions and the electroweak interactions[1]. High-energy e^+e^- colliding beam accelerators have contributed greatly to our knowledge of the gauge particles: first evidence of the gluon for strong interactions was found almost immediately after the turn-on of PETRA from the three-jet events[2], and more recently a first, preliminary determination of the Z^0 mass from the asymmetry in $e^+e^- \to \mu^+\mu^-$ [3]. Theorists have quite precise ideas about the properties of both the Z^0 and the $W^\pm$, which may soon be observed directly at the CERN $p\bar{p}$ Collider.

Unfortunately, we know much less about the mass problem than the gauge problem, especially for particles other than the gauge bosons. An example of this ignorance is our inability to foretell even roughly the mass of the top quark. With this very much in mind, PETRA plans to increase the energy three times in the coming year, first to a center-of-mass energy W = 39 GeV, then to about 41 GeV in early 1983, and finally to 45 GeV next fall. While this mass problem, including the search for Higgs particles[4], will undoubtedly be one of the central concerns of both LEP and SLC, attempts have recently been made to take a first look. These attempts will be discussed in Sec. 7 below.

There are at present the following detectors at PEP and PETRA:

PEP:	DELCO	PETRA:	CELLO
	HRS		JADE
	MAC		MARK J
	MARK II		PLUTO
	TPC		TASSO

At PETRA, CELLO took the place of PLUTO in summer 1982, and PLUTO probably will not be moved into the beam again.

The topics to be covered in this report are:

1. Status of α_s Determination,
2. Precise Measurement of R - TASSO, JADE, MARK J, MARK II, MAC,
3. Measurement of Gluon Spin with High Statistics - TASSO, MARK J,
4. Is Gluon Jet Different from Quark Jet? - JADE, TASSO
5. Particle Identification in Jets,

and 6. Search for Charged Higgs and Technipions from 4-Jet Events - TASSO.

2. STATUS OF α_s DETERMINATION

A. Experimental results

Seven collaborations at PEP and PETRA have determined experimentally the values of the quark-gluon strong coupling constant α_s. Their most recent results are listed in Table 1.

Roughly speaking, α_s is determined by comparing the number of three-jet events with that of two-jet events. As seen from Table 1, however, the situation is more complicated: different values of α_s are obtained when different assumptions are made in analyzing the data. This uncertainty comes mainly from two sources, first whether higher-order corrections in QCD are taken into account, and secondly what assumptions are used in treating the fragmentation of quarks and gluons into hadrons. Except for two recent determinations of α_s by the TASSO and JADE Collaborations to be discussed in Sec. D below, the second-order corrections are not taken into account. The method of energy-energy correlation[12] used by MARK II and MAC is discussed in Sec. B, while the comparison between the independent fragmentation of Hoyer et al.[13] and the Lund fragmentation[14] by CELLO is in Sec. C.

Table 1 - Measured values of the quark-gluon coupling constant α_s at PEP and PETRA

Collaboration	First order in α_s			Second order in α_s ($\overline{MS}$)
	Hoyer et al.	Lund	Energy-energy Correlation	
CELLO[5]	0.15-0.20	0.235-0.28		
JADE[6]	0.20±0.015±0.03			0.16±0.015±0.03
MAC[7]			0.20±0.01±0.02	
MARK II[8]			0.19±0.02±0.03	
MARK J[9]			0.16±0.01	
PLUTO[10]	0.15±0.02±0.03			
TASSO[11]	0.194±0.005±0.03			0.168±0.003±0.03

B. Comments on energy-energy correlation - MARK II, MAC

The energy-energy correlation[12] function is defined by

$$\frac{1}{\sigma_{tot}} \frac{d\Sigma}{d\Omega d\Omega'} = \frac{1}{N} \frac{1}{\Delta\Omega} \frac{1}{\Delta\Omega'} \sum \sum \frac{EE'}{s} \qquad (1)$$

where σ_{tot} is the total hadronic cross section, $s = W^2$, and E and E' are the energies of the particles in the solid angles $\Delta\Omega$ and $\Delta\Omega'$ respectively. The first sum is over all N events, and the second sum is over all pairs of particles in $\Delta\Omega$ and $\Delta\Omega'$. For the purpose of determining α_s, all angles are further summed over except the angle χ between $\Delta\Omega$ and $\Delta\Omega'$, as shown in Fig. 1. The resulting cross section is

$$\frac{1}{\sigma_{tot}} \frac{d\Sigma}{d\cos\chi} = \frac{1}{N} \frac{1}{\Delta \cos\chi} \sum \sum \frac{EE'}{s} \qquad (2)$$

Even as recent as a year ago at the Bonn conference[15], the hope was expressed that this energy-energy correlation function is insensitive to fragmentation, and gives a precise test of QCD. The argument consists essentially of saying that the contributions from quark fragmentation and lepton decay are symmetric under the exchange $\chi \to \pi - \chi$, while the QCD contributions are asymmetric under this exchange.

Recent results from MARK II[8] and MAC[7] show that this independence of fragmentation is not realized. They fitted the energy-energy correlation function of eq. (2) as follows:

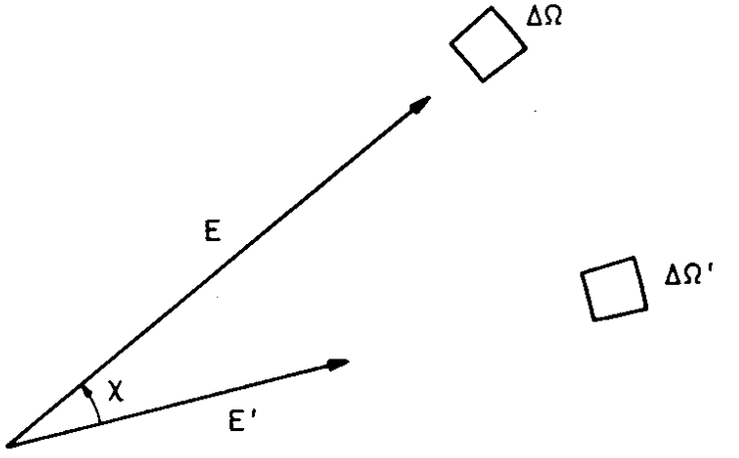

Fig. 1 - Variables for the energy-energy correlation function.

$$\alpha_s F_{QCD}(\chi) + \underbrace{\frac{A_0}{\sqrt{s}}\frac{1}{\sin^3\chi}}_{(q\bar{q}\ \text{frag.})} + \underbrace{\frac{\alpha_s A_1}{\sqrt{s}}}_{(q\bar{q}g\ \text{frag.})} \begin{cases} (\sin\chi)^{-3} & \chi \leq \frac{\pi}{2} \\ 1 + \cos\chi \ \text{(MARK II)} & \chi \geq \frac{\pi}{2} \\ \sin\chi \ \text{(MAC)} & \end{cases} \quad (3)$$

where the first term is given by QCD. While the first correction term due to fragmentation is symmetrical under the exchange $\chi \to \pi - \chi$, the second is not. The MARK II result is shown in Fig. 2, while the one from MAC is in Fig. 3. The fitted results for MARK II are $\alpha_s = 0.19 \pm 0.02$, $A_0 = (0.7 \pm 0.2)$ GeV and $A_1 = (2.6 \pm 0.5)$ GeV, while for MAC $\alpha_s = 0.20 \pm 0.01 \pm 0.02$, $A_0 = (1.2 \pm 0.08 \pm 0.15)$ GeV and $A_1 = (2.5 \pm 0.2 \pm 0.4)$ Gev. For the MARK II analysis, if the asymmetric correction term A_1 due to fragmentation is omitted, then the value of α_s changes from 0.19 to 0.14.

C. Lund vs independent fragmentation - CELLO

To the first order in α_s, there are two diagrams for $e^+e^- \to q\bar{q}g$, as shown in Fig. 4. These QCD diagrams are easy to compute, and give the distributions of the quark, the anti-quark, and the gluon[16]. Unfortunately, neither quark nor gluon is directly observable; instead they are fragmented into hadrons. Therefore, in order to compare the QCD predictions with the experimental data, a model is needed for this complicated fragmentation process.

Fragmentation was first studied by Field and Feynman[17] in the context of two-jet events $e^+e^- \to q\bar{q}$, and the generalization to the

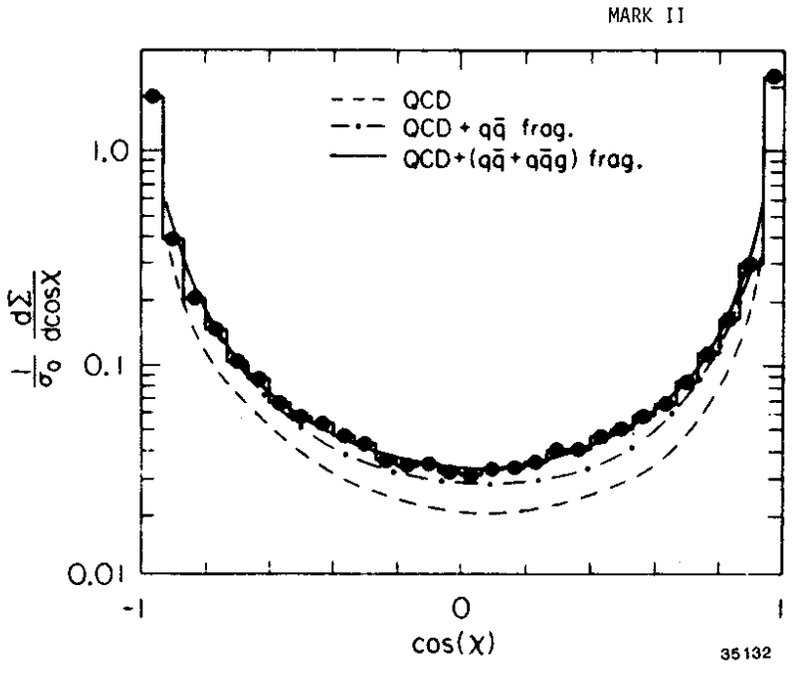

Fig. 2 - $(1/\sigma_0)d\Sigma/d\cos\chi$ as a function of $\cos\chi$. The size of the dots corresponds to the statistical errors. The dashed line is the QCD prediction. The dash-dotted line is the QCD result plus the $q\bar{q}$ fragmentation term. The solid line is the sum of the QCD predictions and the two nonperturbative contributions - MARK II.

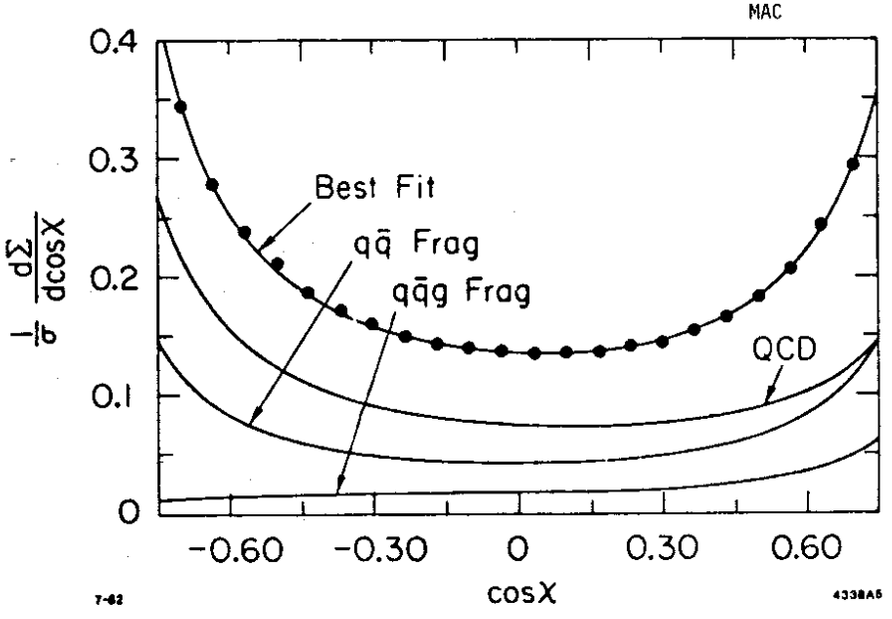

Fig. 3 - The full experimental energy-energy correlation as a function of $\cos\chi$, the correlation angle. Also shown are the fitted contributions from QCD, the $q\bar{q}$ and the $q\bar{q}g$ fragmentation terms - MAC.

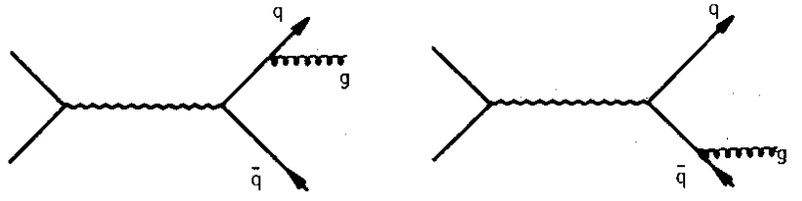

Fig. 4 - Diagrams for $e^+e^- \to q\bar{q}g$ to order α_s.

three-jet events through $e^+e^- \to q\bar{q}g$ was first carried out by Hoyer, Osland, Sander, Walsh and Zerwas[13]. In both of these Monte Carlos, the jets fragment independently, as schematically shown in Fig. 5(a). The Lund group of Andersson, Gustafson, and Sjoestrand[14] had the idea of combining fragmentation with the concept of the color string, which is stretched from the quark via the gluon to the anti-quark. This color string is envisaged to break first to produce a hadron carrying a sizable fraction of the gluon energy. The remainder of the gluon energy is then shared between the two pieces of the broken string, which are fragmented independently in their respective center-of-mass systems[14]. This Lund fragmentation process is shown schematically in Fig. 5(b).

There is no compelling argument to prefer one of these two fragmentation models over the other. While the use of the color string has its appeal, it must be emphasized that there are many more parameters in the Lund model than in the model of Hoyer et al. Under this circumstance, it is of importance to ascertain whether there is significant dependence of the α_s determination on the fragmentation model.

This problem has been studied by both the CELLO[5] and the JADE[6] Collaborations. Their analyses reached different conclusions. JADE used both fragmentation models[13,14] to determine the corrected x_1 and x_T distributions, where $x_T = x_2 \sin\theta_{12}$. They found that "the corrections are, within the errors, independent of the fragmentation scheme used". On the other hand, CELLO found that, depending on the distribution used, the Lund model gives α_s

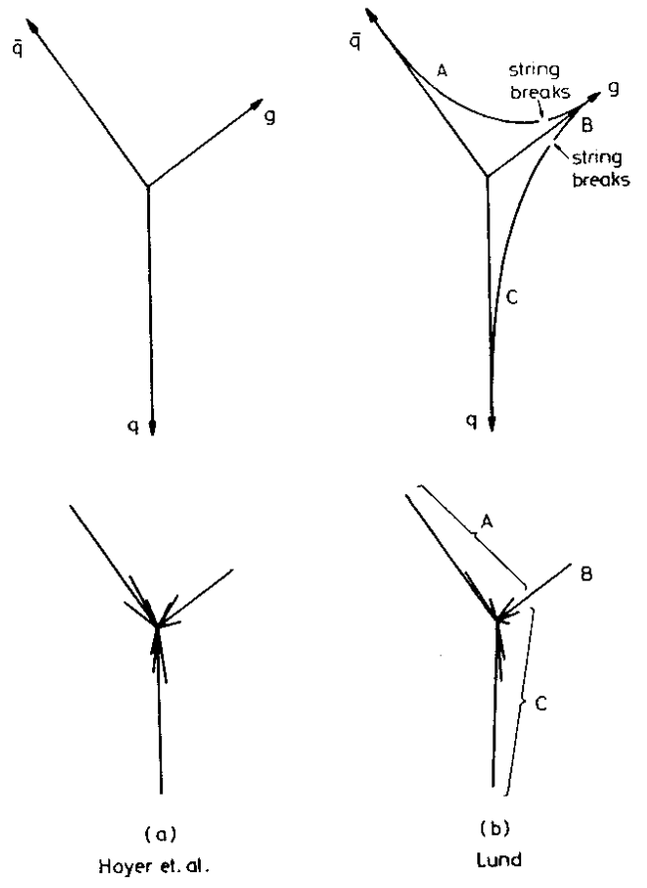

Fig. 5 - Schematic representation of fragmentation models.

between 28% to 67% higher than the model of Hoyer et al. The two extreme cases are:

Smallest difference: three-jet fraction from events with oblateness larger than 0.3

Lund $\alpha_s = 0.255 \pm 0.050$

Hoyer $\alpha_s = 0.200 \pm 0.035$ ratio = 1.28

Largest difference: energy-energy correlation function

Lund $\alpha_s = 0.25 \pm 0.04$

Hoyer $\alpha_s = 0.15 \pm 0.02$ ratio = 1.67

In particular, this result from CELLO implies that, contrary to the earlier hope as described in Sec. B, the energy-energy correlation function is sensitive to fragmentation.

In order to have a better understanding of this rather significant dependence on fragmentation, CELLO has attempted various modifications and combinations of the Monte Carlo programs. The result is shown in Fig. 6. It is seen that about two thirds of the difference is due to the different fragmentation schemes used (quark, gluon independent fragmentation scheme as in Hoyer et al. model versus the string fragmentation scheme as in the Lund model).

D. α_s determination in second order - TASSO, JADE

As shown in Table 1, the determination of α_s has been carried out in both first order and second order. In first order, the only QCD diagrams taken into account for $e^+e^- \to q\bar{q}g$ are the two shown in Fig. 4. In second order, it is necessary to consider in addition not only the

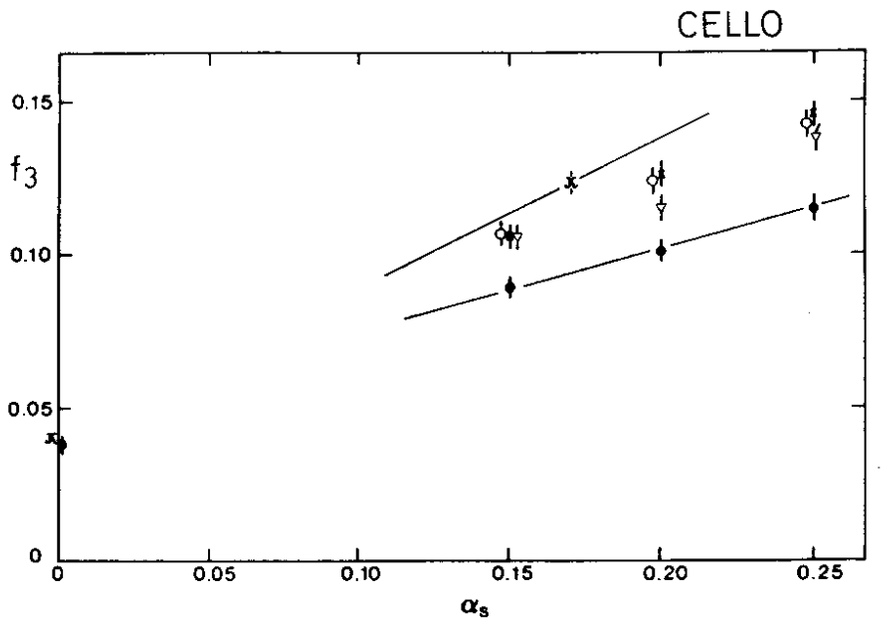

Fig. 6 - CELLO Monte Carlo study of the three-jet fraction f_3 versus α_s for different fragmentation conditions (S>0.25, A<0.10):

- ● Lund Model $\sigma_q = 0.30$ GeV/c V/(P+V) = 0.5
- x Lund program with FF fragmentation and gluon as a quark $a_g = a_f = 0.77$
- o idem but $a_g = 1$
- ▽ Lund program FF fragmentation but gluon as in LM
- x Hoyer Model with $\sigma_q = 0.30$ GeV/c.

diagrams of Fig. 7 for $e^+e^- \to q\bar{q}g$ but also those in Fig. 8 for $e^+e^- \to q\bar{q}gg$ and $e^+e^- \to q\bar{q}q\bar{q}$. This theoretical analysis was carried out by three groups: R. K. Ellis et al.[18], Fabricius et al. (FKSS)[19], and Vermaseren et al.[20]. Although all three groups studied the same diagrams, and used the same renormalization scheme, their results were in apparent conflict. FKSS has found the α_s^2 corrections to be of reasonably small size, but the other two groups have concluded that the α_s^2 corrections are comparable to the α_s terms, making it necessary to study α_s^3 corrections (which is virtually hopeless because of the large number of diagrams involved). Fortunately, this discrepancy has been understood[21] as due to different definitions of thrust and hence the three-jet events. With this understanding, it is now possible to carry out second-order determination of α_s provided that the FKSS result, rather than those of the other two groups, is used. This has been accomplished by the TASSO and JADE Collaborations.

The method used by TASSO[11] is as follows. The FKSS formulas are built in the event generator, and independent Field-Feynman (FF) fragmentation is used. The TASSO data from ρ^0 production[22] is used to fix one of the Field-Feynman parameters on the ratio of pseudoscalar to vector mesons P/V. With this ratio fixed, the second-order α_s together with the other two Field-Feynman parameters are found by fitting simultaneously the experimental data. Four distributions are used, namely those in the average transverse momentum out of the event plane $\langle p_{T_{out}}^2 \rangle$, in sphericity S, in planarity, and in the momentum fraction $x = P_h/E_{beam}$ for $x > 0.3$. In terms of the normalized eigenvalues Q_1, Q_2 and Q_3 of

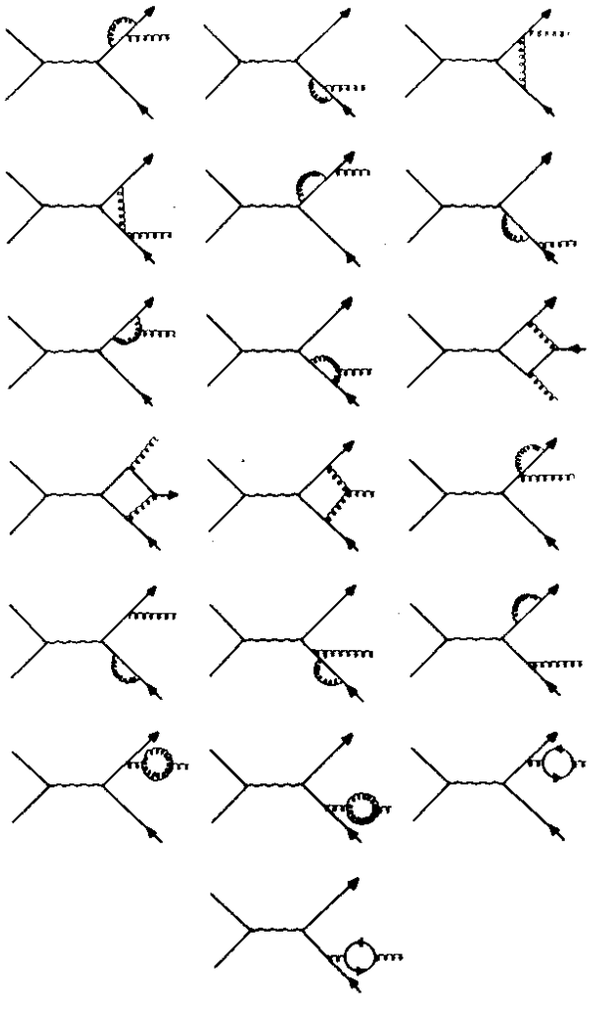

Fig. 7 - Diagrams for $e^+e^- \to q\bar{q}g$ to order α_s^2.

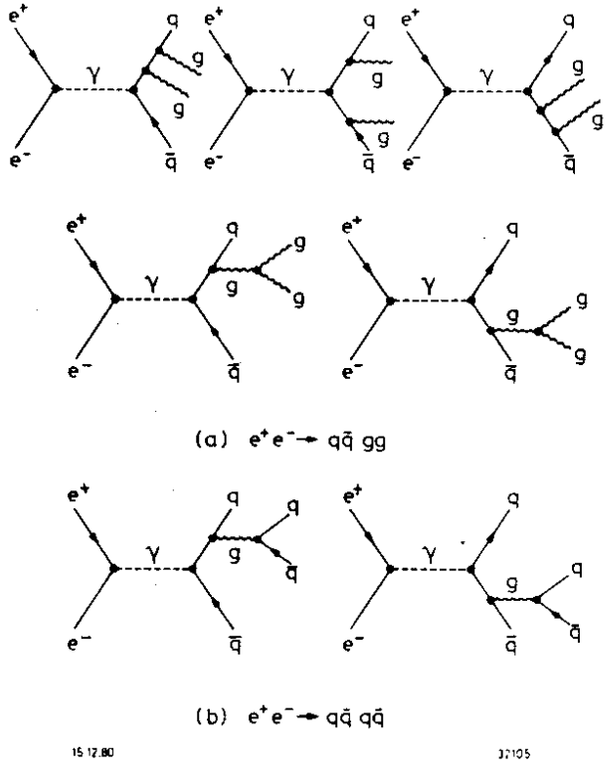

Fig. 8 - Diagrams for $e^+e^- \to q\bar{q}gg$ and $q\bar{q}q\bar{q}$ to order α_s^2 (lowest order).

the momentum tensor[11], the sphericity $S = \frac{3}{2}(Q_1 + Q_2)$ and the planarity = $Q_2 - Q_1$. The resulting second-order α_s, as already given in Table 1, and the three Field-Feynman parameters are

$\alpha_s = 0.168 \pm 0.003$ (stat.) $\pm$ 0.03 (sys.)

$\sigma_q = (0.350 \pm 0.003 \pm 0.02)$ GeV/c

$a_F = 0.70 \pm 0.01 \pm 0.10$

and $\frac{P}{P+V} = 0.42$ from ρ^0 production, (see Sec. 6 below)

where σ_q describes the transverse momentum distribution and a_F the longitudinal momentum distribution for quark fragmentation. The systematic errors are valid only in the context of the Field-Feynman fragmentation model.

If the same procedure is applied to determinate the first order α_s, the corresponding results are

$\alpha_s = 0.194 \pm 0.005$ (stat.) $\pm$ 0.03 (sys.)

$\sigma_q = (0.358 \pm 0.003 \pm 0.02)$ GeV/c

$a_F = 0.70 \pm 0.02 \pm 0.10$

The comparison of the two fits with the TASSO experimental data is shown in Figs. 9 - 12. It is seen that these event shape distributions are well fitted by either first order or second order in α_s. The resulting values of α_s are of course not the same, the second-order result being 13 % lower. It is important that the analysis is carried out with simultaneous fits. Obviously, if the second-order value for α_s were used in a first-order fit, or vice versa, the resulting fits would be very poor. In order to establish the need of second-order in α_s, the above parameters should be used for the purpose of comparing some other distribution, preferably one related to four-jet events.

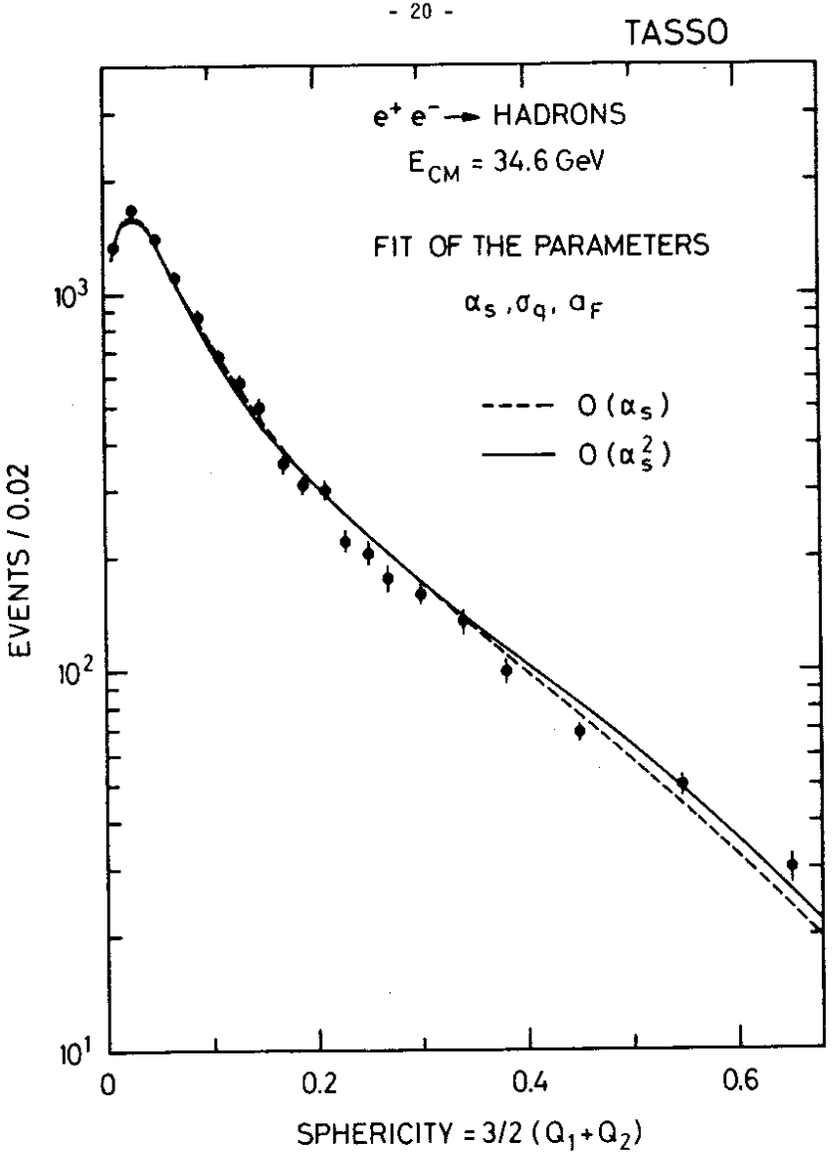

Fig. 9 - Sphericity distribution from TASSO. The dashed line and the solid line are respectively the results of the simultaneous fits in first-order and second-order QCD with Field-Feynman fragmentation.

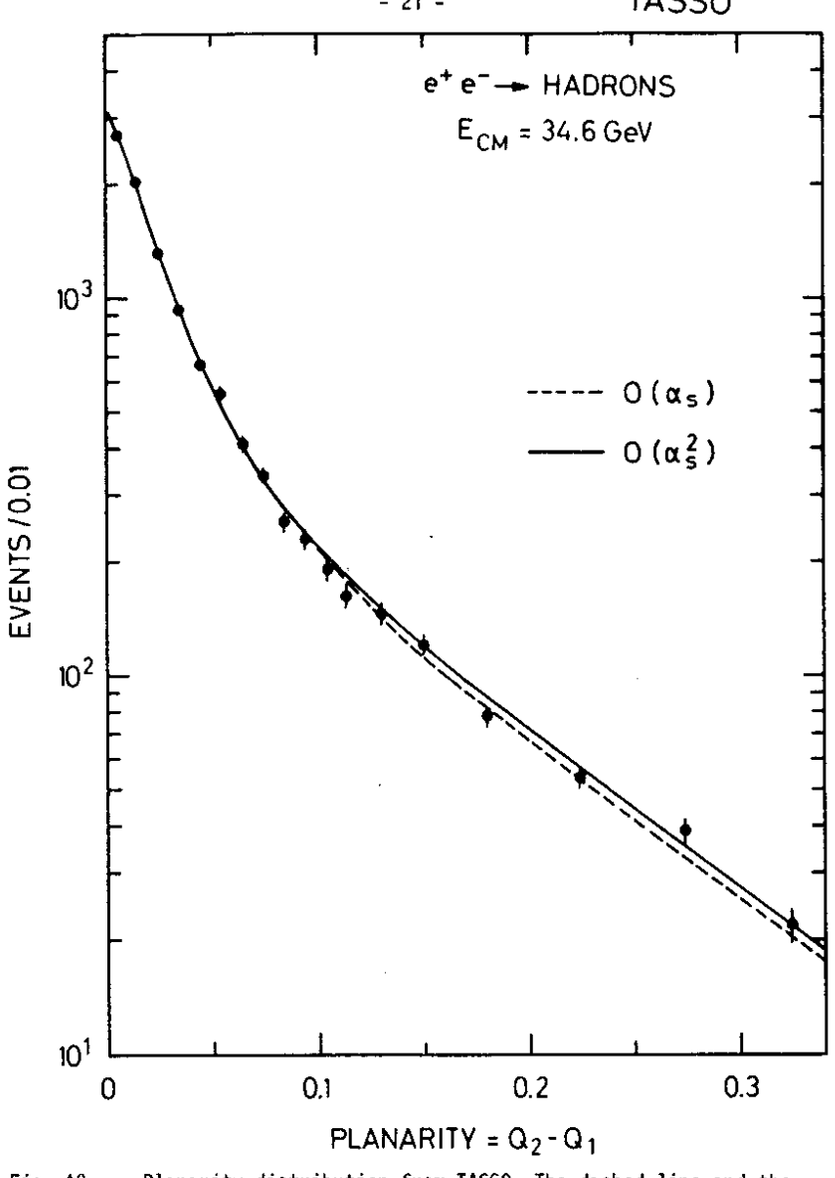

Fig. 10 - Planarity distribution from TASSO. The dashed line and the solid line are respectively the results of the simultaneous fits in first-order and second-order QCD with Field-Feynman fragmentation.

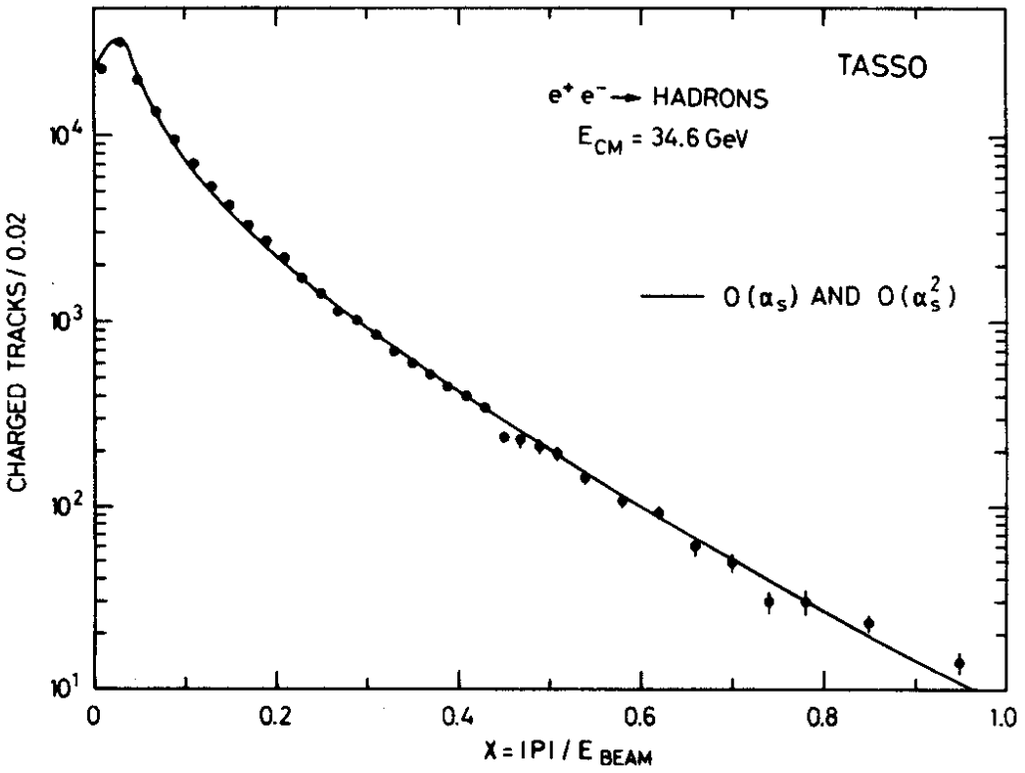

Fig. 12 - TASSO inclusive distribution in x, the momentum fraction of the charged hadrons, from TASSO. In this case the first-order and second-order results are indistinguishable.

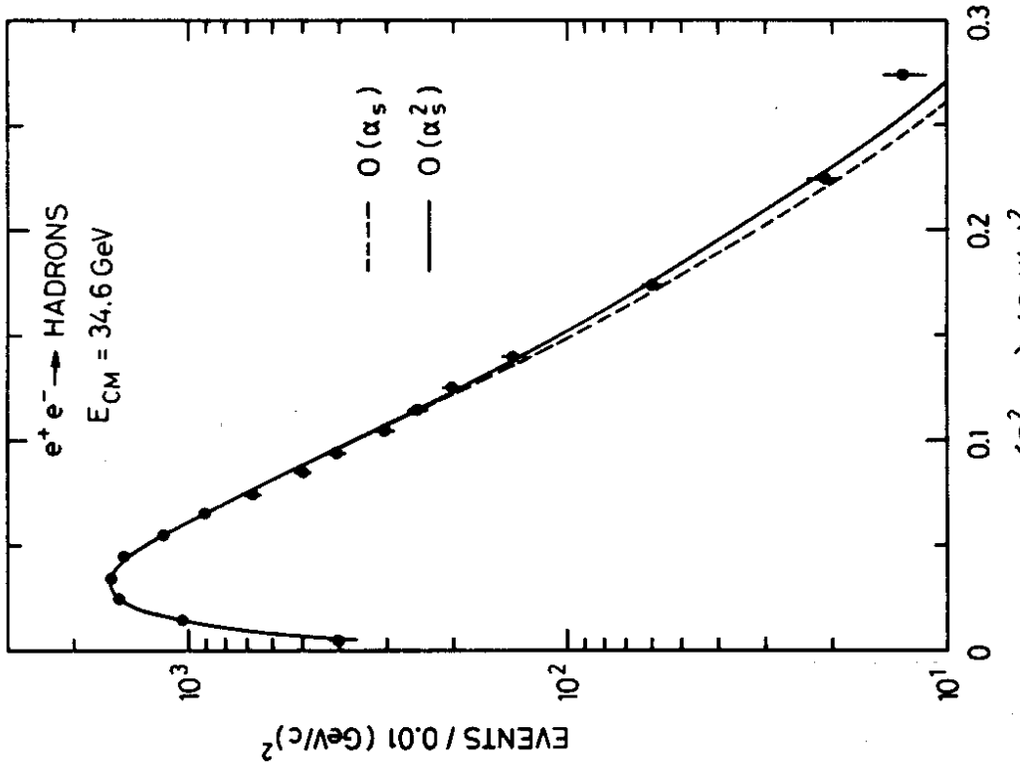

Fig. 11 - TASSO distribution in $\langle p_T^2 \text{ out} \rangle$, the average transverse momentum out of the event plane. The dashed line and the solid line are respectively the results of the simultaneous fits in first-order and second-order QCD with Field-Feynman fragmentation.

The method used by JADE[6] is similar but not identical. The distribution in the parton thrust x_1 is shown in Fig. 13. Both independent fragmentation via Hoyer et al. and Lund fragmentation are used, and the value given in Table 1 is the average of these two fragmentation models.

A comparison of the second-order values of α_s from TASSO and JADE with the corresponding first-order results shows that there is a reduction of 13% to 20% in going from first order to second order.

3. PRECISE MEASUREMENT OF R - TASSO, JADE, MARK J, MARK II, MAC

R for the total hadronic cross section is defined as the ratio

$$R = \frac{\text{total cross section for } e^+e^- \to \text{hadrons}}{\text{total cross section for } e^+e^- \to \mu^+\mu^-} \qquad (4)$$

at the same energy. More precisely, the denominator is not the actual total cross section for $e^+e^- \to \mu^+\mu^-$, but rather the theoretical total cross section in the lowest-order QED without weak interactions. Therefore

$$R = \frac{s \text{ in GeV}^2}{86.856} \text{ (total cross section for } e^+e^- \to \text{hadrons in nb).} \qquad (5)$$

The precise determination therefore involves the careful identification of hadronic events, subtraction of backgrounds, calculation of acceptance, measurement of luminosity etc., but not any experimental determination of the total cross section for μ pair production.

The results of the recent measurements of R by various collaborations are listed in Table 2. So far, only the TASSO[23] value is published. The two values given by MAC[7] differ only in the method of analysis. Figure 14 gives an overall view [26] of the measured values of R from low energies to the highest available energy.

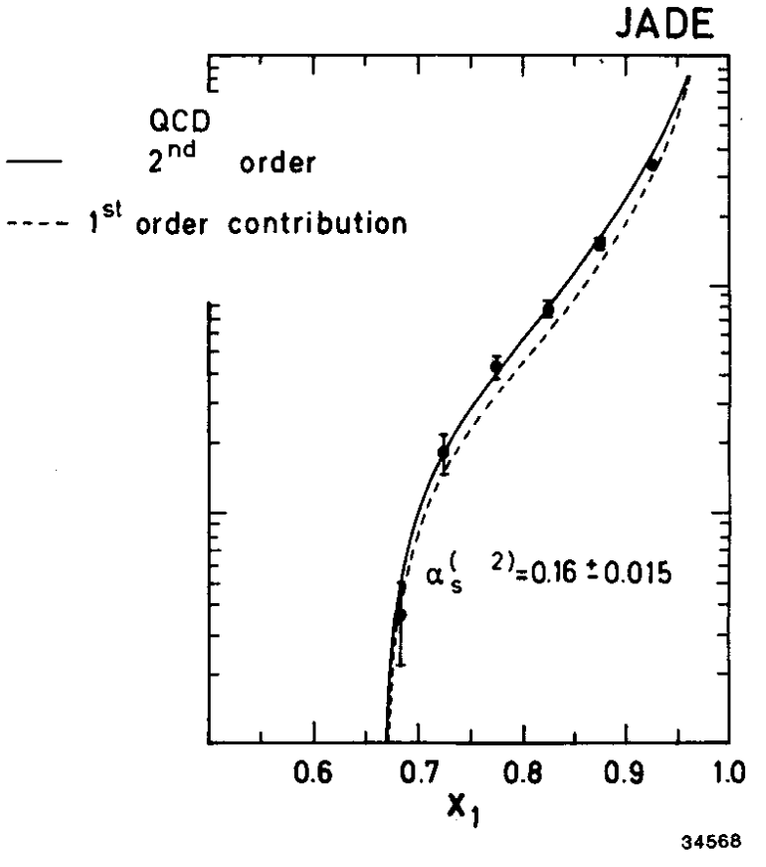

Fig. 13 - The corrected x_1 distribution together with the second-order QCD best fit. The first-order contribution of this fit is indicated by the broken curve. The fit did not include data above $x_1 = 0.85$ - JADE.

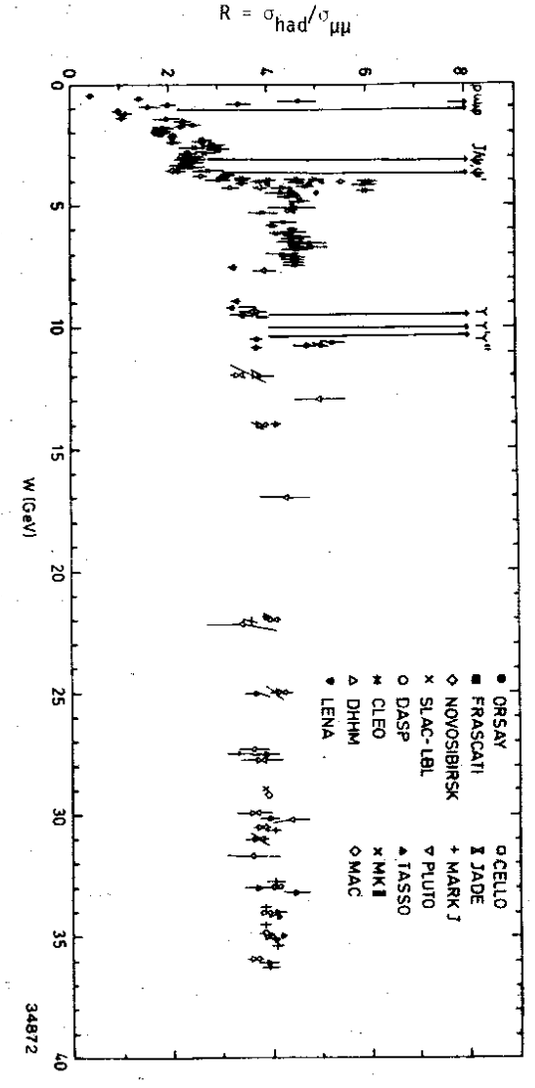

Fig. 14 - Overall view of the measured values of R for hadronic total cross sections from low energies to the highest available energy.

Table 2 - Measured values of R for total hadronic cross section at PEP and PETRA.

Collaboration	Range of center-of-mass energy in GeV	$R \pm \Delta R_{stat} \pm \Delta R_{sys}$
TASSO[23]	14.0 - 36.7	4.01 ± 0.03 ± 0.20
JADE[24]	14.0 - 36.7	3.93 ± 0.03 ± 0.09
MARK J[9,24]	12.0 - 36.7	3.84 ± 0.05 ± 0.22
MARK II[25]	29.0	3.90 ± 0.05 ± 0.25
MAC[7]	29.0	3.93 ± 0.04 ± 0.12 3.87 ± 0.04 ± 0.10

Since the JADE[24] value is the most accurate one in the energy range of PEP and PETRA, it is described in this section. The various contributions to the systematic error of JADE are shown in Table 3. When added in quadrature, the total is 3%. In Fig. 15 (a) and (b), the measured distributions in the number of charged prongs and the momentum balance along the beam direction are compared with the Monte Carlo simulation. In Fig. 15 (c), the distribution of the vertex along the beam direction is given. In all three cases, the cuts used are also shown and are quite far in the tails of the distributions.

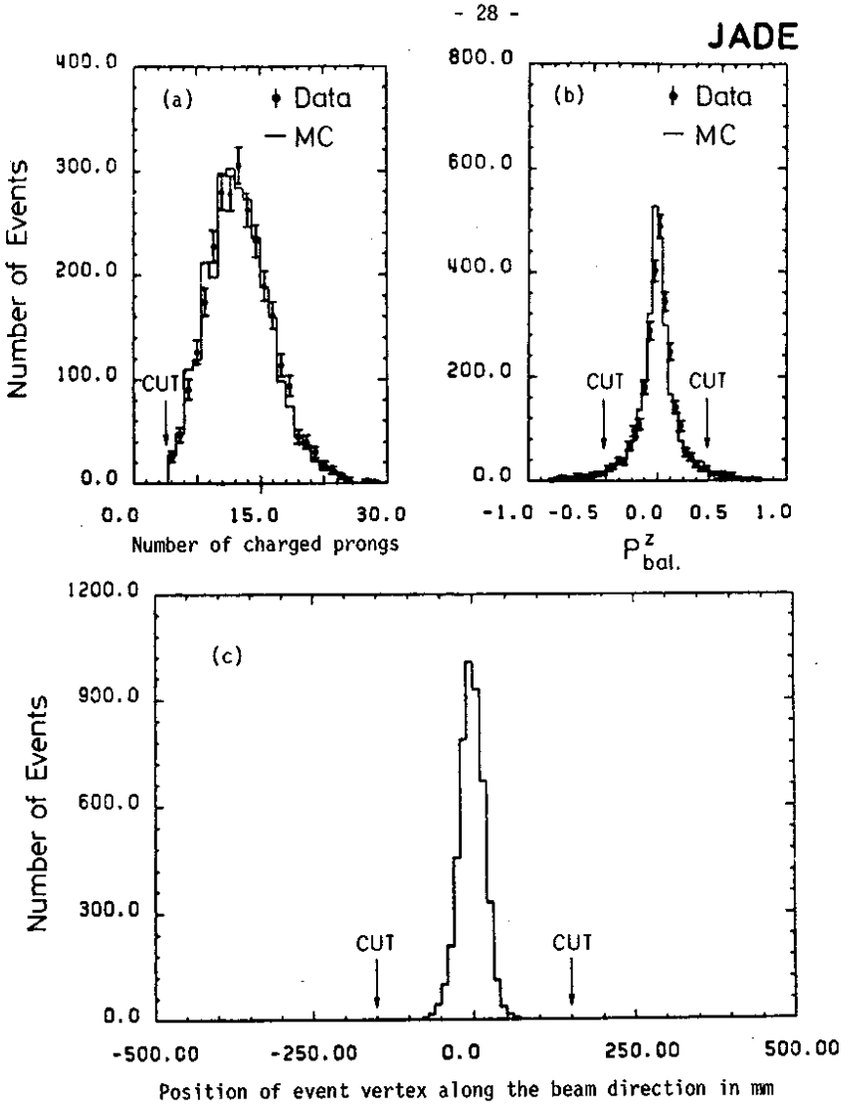

Fig. 15 - Some JADE acceptance cuts for hadronic events.

Table 3 - Contributions to the systematic error of the JADE precise measurement of R for total hadronic cross section.

	Systematic error (ΔR) E_{cm} 22 - 36.7 GeV
Background: $N_{\tau\tau}$ (2.4% ± 1.4%) low E_{cm} $N_{\gamma\gamma}$ (0.5 ± 0.5%) high E_{cm} $N_{\gamma\gamma}$ (0.7 ± 0.5%) $\sum$	± 1.6%
Acceptance (85% w/o rad corr.)	± 1.5%
Luminosity (barrel Bhabhas)	± 1.8%
Radiative correction (α^3) 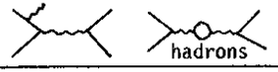	± 0.8%
Higher order radiative corr.	No error for higher order corr. included
Total $\sum$	± 3.0%

In order to remove the background from two-photon processes

$$e^+e^- \to e^+e^- \text{ hadrons}$$

with the e^+ and the e^- in the final state going near the beam directions and hence not detected, a cut is introduced in the total visible energy, where the total visible energy is the sum of energies carried by the charged tracks and the photons. As functions of the ratio of the total visible energy to the beam energy, the observed distributions, the Monte Carlo simulation, and the cuts used are all shown in Fig. 16. The peak

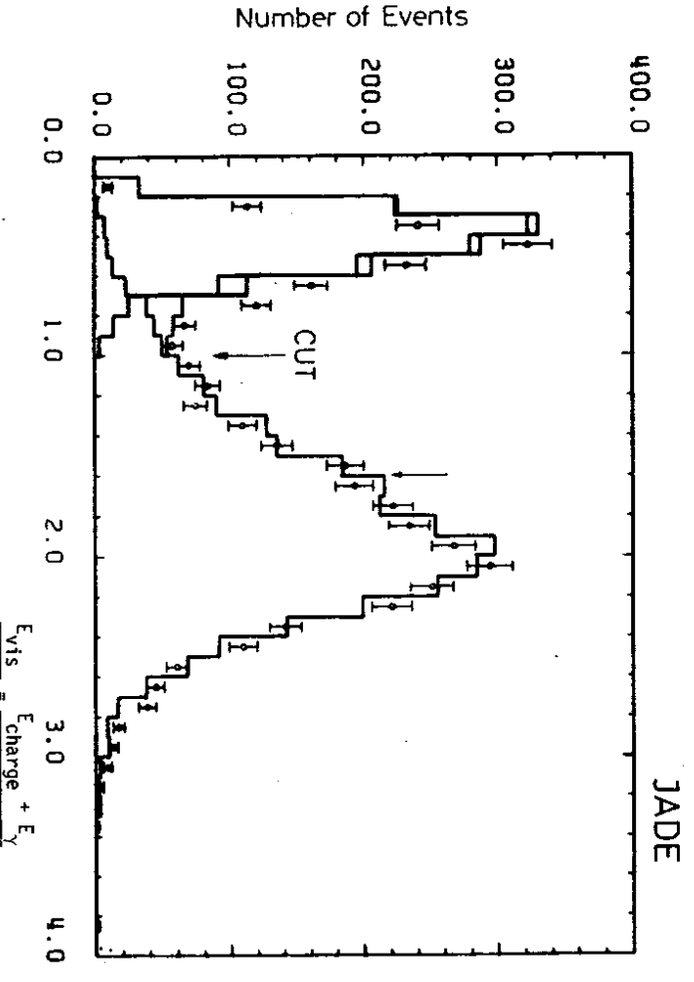

Fig. 16 - JADE acceptance cut in the ratio of the visible energy to the beam energy.

on the right is due to the hadronic events of interest, while that on the left is due to two-photon processes. Because of the good agreement between the experimental data and the Monte Carlo simulation, changing the position of the cut has relatively little effect on the value of R. For example, even with the rather extreme cuts at 1.0 and 1.6, as shown in Fig. 16, R changes by less than one per cent.

JADE has an accurate measurement of the luminosity. This is accomplished not by the small-angle luminosity monitors, but by the observation of Bhabha events in the barrel shower counters. The data, the Monte Carlo, and the cut used are shown in Fig. 17.

As functions of energy, the TASSO[23] and JADE[24] results on R are shown in Fig. 18 and Fig. 19 respectively.

One of the main motivations for the precise measurement of R for hadronic total cross section is that R as a function of the center-of-mass energy gives unambiguous determination, independent of fragmentation, of the quark-gluon coupling constant α_s and the Weinberg angle Θ_W for electroweak interaction. This extraction of these two fundamental constants from the data on R is carried out differently by the TASSO and JADE Collaborations. TASSO performed a simultaneous fit to the data by varying α_s and Θ_W, and obtained[23]

$$\alpha_s = 0.18 \pm 0.03 \pm 0.14 \quad \text{for} \quad s = 1000\ \text{GeV}^2$$

and $$\sin^2\Theta_W = 0.40 \pm 0.16 \pm 0.02.$$

The resulting R with these parameters are shown as the solid line in Fig. 18. On the other hand, JADE fitted each parameter separately with the other one held fixed. The results are[24]

If $\sin^2\Theta_W = 0.228$ is assumed, then $\alpha_s = 0.14 \pm 0.08$ at $s = 900\ \text{GeV}^2$;

if $\alpha_s = 0.18$ is assumed at $s = 900\ \text{GeV}^2$, then $\sin^2\Theta_W = 0.25 \pm 0.05$.

In both cases, systematic errors are included.

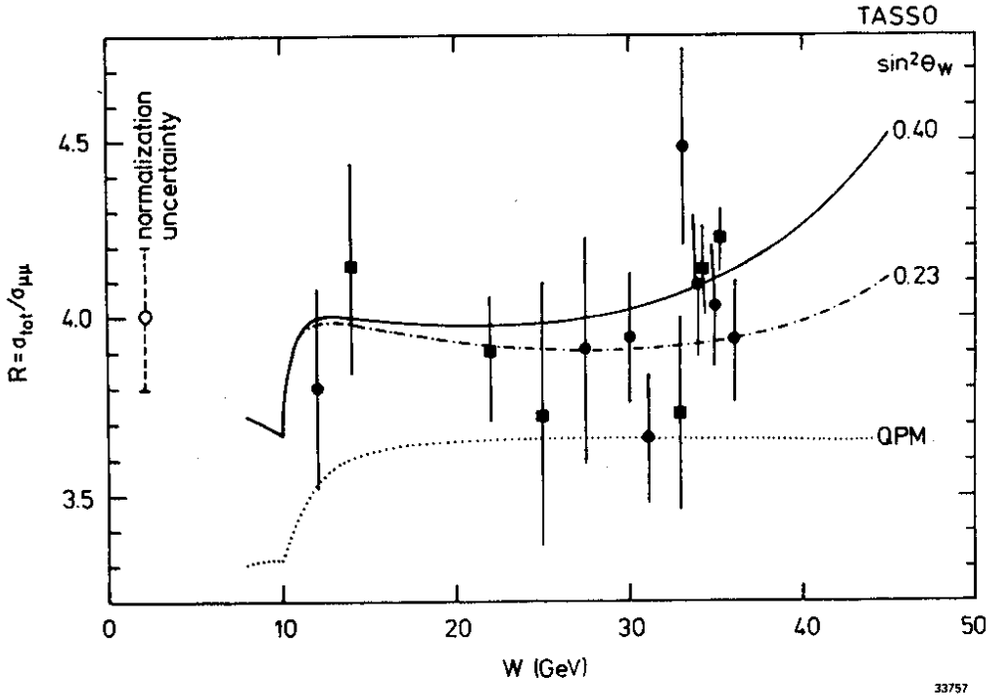

Fig. 18 - TASSO results on R for total hadronic cross section. The points marked by a circle are from the runs in 1979 and 1980, while those marked by a square from 1981. The errors shown include the statistical and point-to-point systematic uncertainty, while the overall normalization uncertainty is indicated separately on the left. The dotted line shows the expectation from the quark parton model (QPM). The full line represents the best fit including weak contributions, while the dashed-dotted line was computed with $\alpha_s(s = 1000\ GeV^2) = 0.18$ and $\sin^2\theta_W = 0.23$

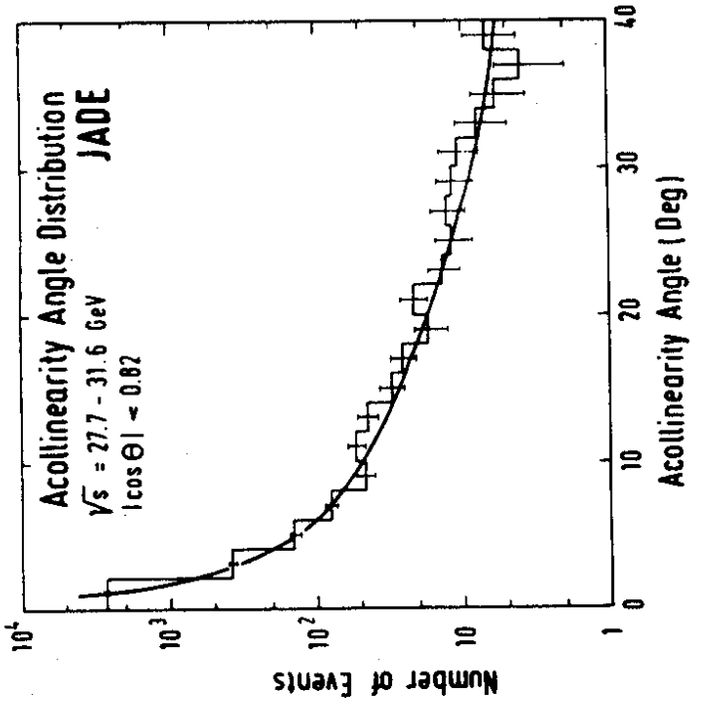

Fig. 17 - JADE luminosity measurement from Bhabha scattering.

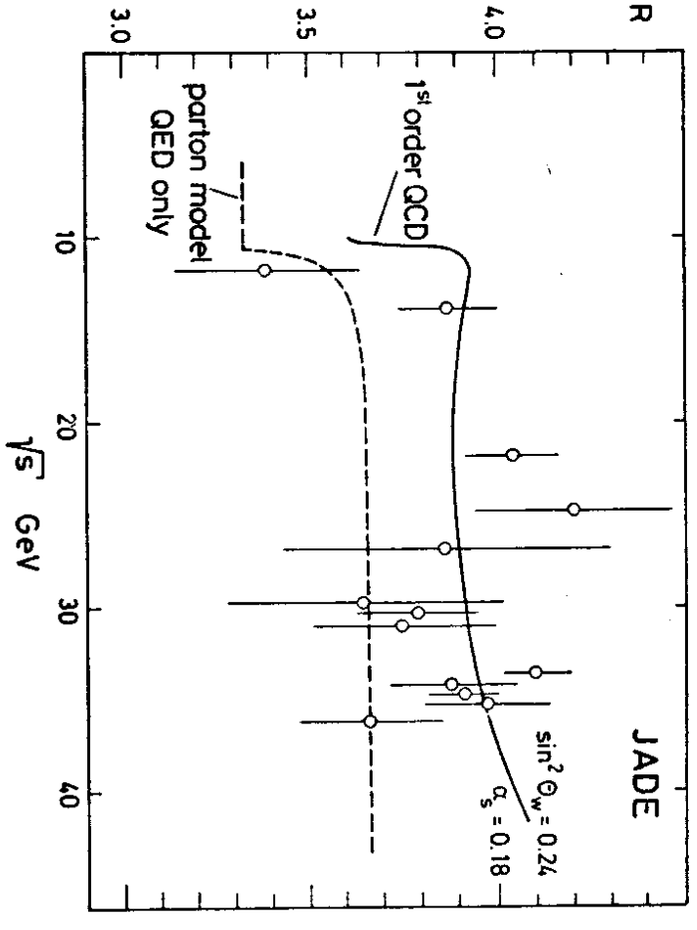

Fig. 19 - JADE results on R for total cross section. The dashed line shows the expectation from the quark parton model, while the solid line is computed with $\alpha_s = 0.18$ and $\sin^2\Theta_W = 0.24$.

4. MEASUREMENT OF GLUON SPIN WITH HIGH STATISTICS - TASSO, MARK J

Since QCD is a gauge theory, its gluon must have spin 1. Experimentally, the gluon spin being 1 was first verified by TASSO[27] in 1980, and similar conclusions have been reached also by PLUTO[28] and CELLO[29]. With the high statistics available now, TASSO[30] and MARK J[9] have recently repeated the measurement of the gluon spin.

During my talk here last year, the method used by TASSO was described in some detail[31]. Exactly the same method is used with the high statistics. Briefly, let

$$x_j = E_j/E_{beam},$$

where E_j is the energy of jet j, j = 1, 2, 3. With the three x's arranged in the order

$$x_3 < x_2 < x_1,$$

the Ellis-Karliner angle is given by[32]

$$|\cos\tilde{\Theta}| = \frac{x_2 - x_3}{x_1}. \qquad (6)$$

TASSO applied three-jet analysis to 16,000 hadronic events, and computed the x's from the angles between the jet directions. 1600 events survive after a cut of $x_1 < 0.9$, which implies a minimum angle of 70° between the jets. In Fig. 20, these events are plotted as a function of the Ellis-Karliner angle, and compared with the Monte Carlo predictions under the two assumptions of spin 1 and spin 0. Spin 0 is clearly ruled out.

Instead of $|\cos\tilde{\Theta}|$, the ratio $x_3^2/(x_1^2 + x_2^2)$ was used by MARK J[9]. Their result is shown in Fig. 21, and, for 9 degrees of freedom, the χ^2 is 10.5 for spin 1 and 98.1 for spin 0.

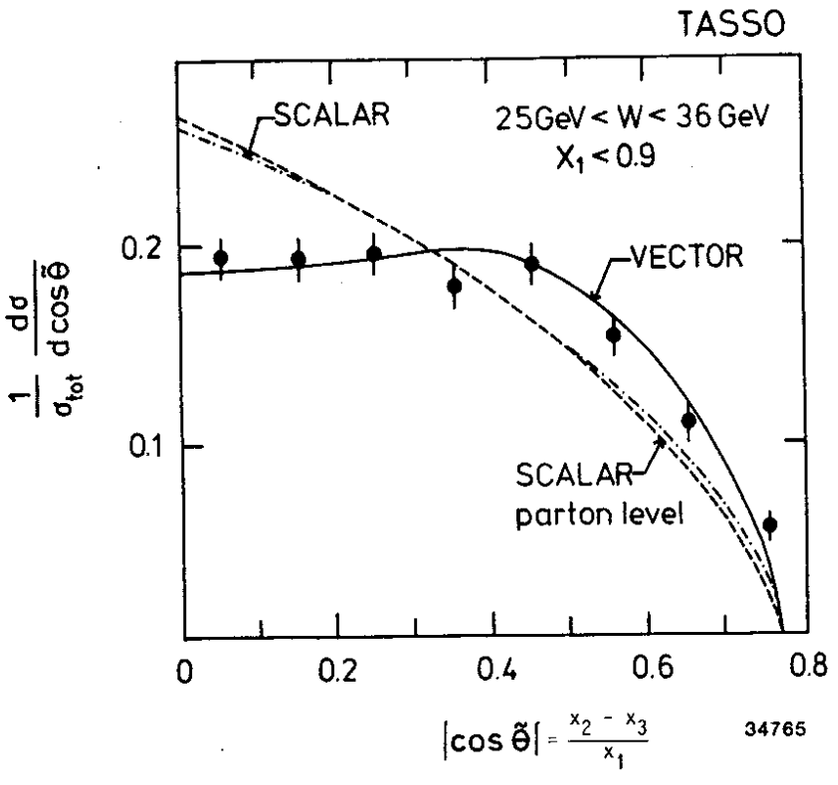

Fig. 20 - Observed distribution of the TASSO data in the region $x_1 < 0.9$ as a function of the Ellis Karliner angle $\tilde{\theta}$. The solid line shows the QCD Monte Carlo prediction, dashed line the prediction for the scalar gluons (– – – for Monte Carlo scalar model; —·— for scalar model of parton level). All curves are normalized to the number of observed events.

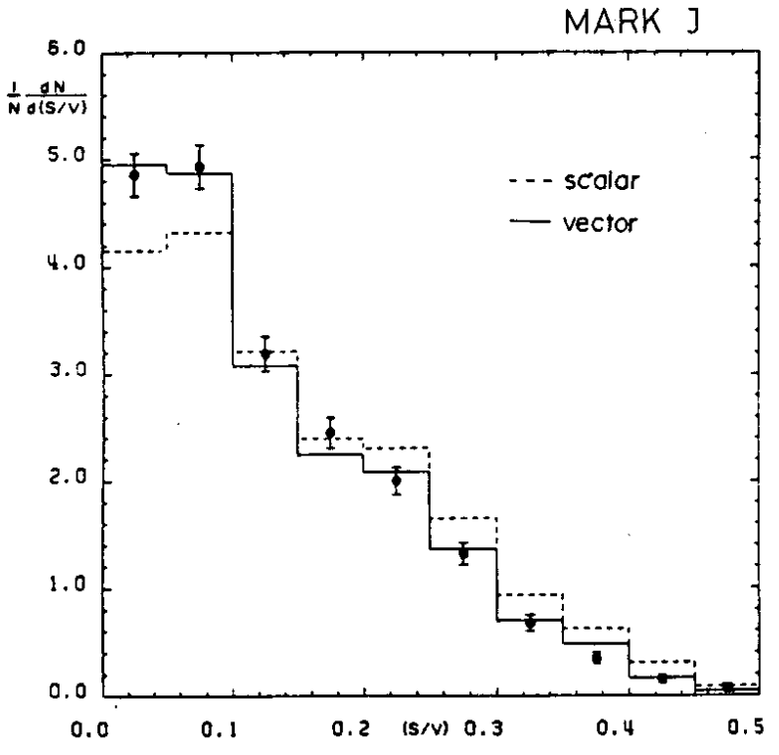

Fig. 21 - Observed distribution of the MARK J data as a function of the variable $x_3^2/(x_1^2 + x_2^2)$. The solid line shows the QCD Monte Carlo prediction, and the dotted line the prediction for scalar gluons.

5. IS GLUON JET DIFFERENT FROM QUARK JET? - JADE, TASSO

A. Average transverse momentum - JADE

A year ago at this Topical Conference, I reported[31] the preliminary result from JADE showing differences between quark and gluon jets. Briefly, their result at that time was as follows. Take the three-jet events and arrange the jets according to energy as described in the preceding section. By Monte Carlo calculation using the Lund model[14], it is found that for W = 33 GeV in 51% of the events jet 3 is the gluon jet; 22% jet 2 is the gluon jet; 12% jet 1 is the gluon jet; and 15% the event is actually a two-jet event without a gluon jet. The JADE experimental result is that, for the same visible energy, the average transverse momentum $\langle p_T \rangle$ is larger for jet 3 than for jets 1 and 2. The question was raised whether this effect was due to the use of the visible jet energy as the variable.

JADE has now carried out this analysis[24,33] using instead the jet energies calculated from the angles between the jets. Fig. 22 shows, on the basis of model calculations at W = 33 GeV, the probability η_j for jet j being closest to the gluon direction as a function of the jet energy. Note that

$$W/3 \leq E_1 < W/2$$

$$W/4 \leq E_2 < W/2$$

and

$$E_3 \leq W/3 \ .$$

Therefore, for any given W, the overlap between E_1 and E_2 is from W/3 to W/2, that between E_2 and E_3 from W/4 to W/3, but E_1 and E_3 never overlap.

On the basis of 2048 planar 3-jet events (out of 18424 hadronic

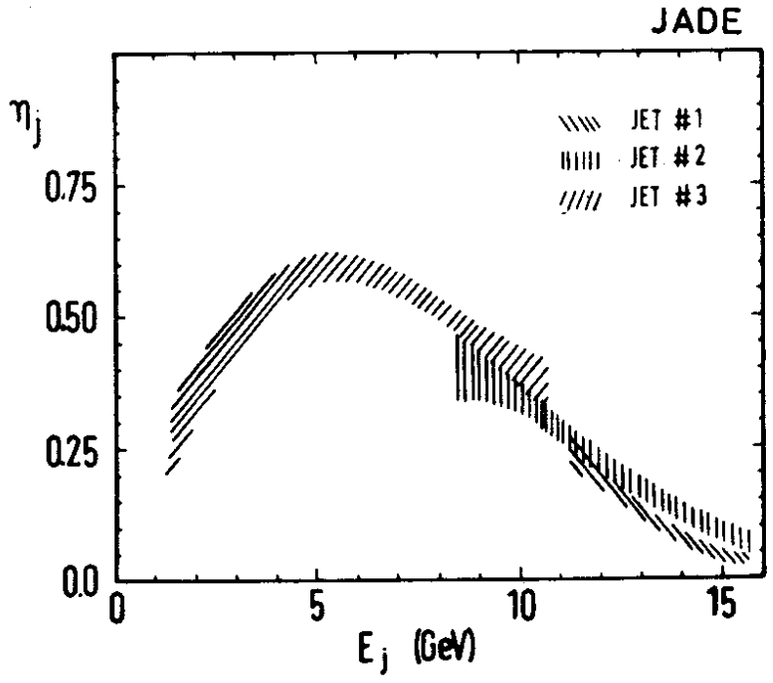

Fig. 22 - The probability η_j for jet j being closest to the gluon direction as a function of the reconstructed jet energy E_j obtained from model calculations at a fixed c.m. energy of 33 GeV. The widths of the shaded areas indicate the statistical errors.

events) at W between 29 and 36.4 GeV and 307 planar 3-jet events (out of 1945 hadronic events) at W = 22 GeV, the JADE result for the average transverse momenta of a jet is shown in Fig. 23(a). The g = q model calculation using Hoyer et al.[13] shown in Fig. 23(b) does not indicate any larger transverse momentum for jet 3, indicating that there is no significant bias in the selection of events. The experimentally observed larger transverse momentum for jet 3 can be reproduced by increasing the σ_q for the gluon from 330 MeV/c to 500 MeV/c (independent of energy), or by using the Lund model[14]. In this Fig. 23, the overlaps of the energy ranges for the three jets are much more than those kinematically allowed for any given W, as discussed in the preceding paragraph and Fig. 22. The reason is of course that the values of W ranges from 22 GeV to 36.4 GeV. In particular, the five data points indicated by arrows in Fig. 23(a) are from W = 22 GeV. Accordingly, as emphasized by the JADE Collaboration, the comparison is made between jet 3 at W = 29 to 36.4 GeV and jet 2 at W = 22 GeV. For this comparison, jet 3 has significantly larger average transverse momentum than jet 2 for the same jet energy.

In this comparison, it is assumed that, at the relatively low energy of W = 22 GeV, three-jet analysis is capable of identifying correctly the hadrons in the three jets. Note that a higher percentage of hadronic events at W = 22 GeV (307/1945 = 16%) is classified as three-jet events than at W = 29 - 36.4 GeV (2048/18424 = 11%). To avoid this assumption, JADE has carried out an alternative analysis[24,34] comparing jet 3 at the higher W with the quark jets from the two-jet events at W = 14 GeV. For the purpose of this comparison, the trans-

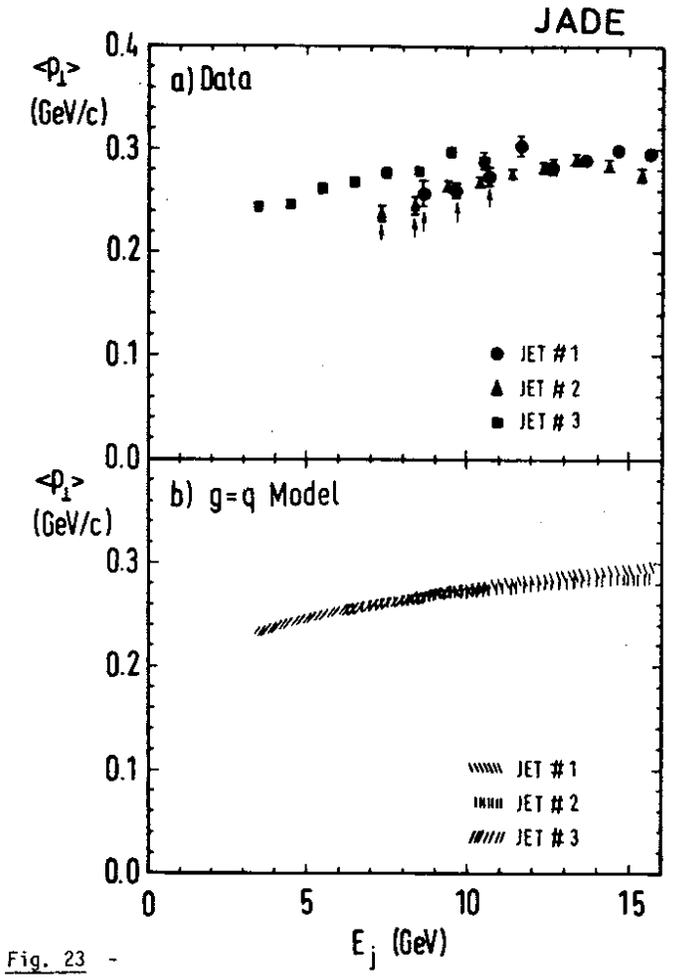

Fig. 23 - Average p_T distribution from JADE for the highest energy jets(E_1), medium energy jets (E_2), and lowest energy jets (E_3) as a function of the jet energy E_j calculated from the angles between the three jets. The center-of-mass energy is between 22 and 36.7 GeV. Fig. 20(a) is from the experimental data, where the arrows indicate the data points at W = 22 GeV. Fig. 20(b) is the prediction of the q = g Monte Carlo model.

verse momentum is calculated using only particles produced within 50° of the reconstructed jet axes, as shown in Fig. 24. The result of this comparison is shown in Fig. 25, both for the result of the Monte Carlo of Hoyer, Osland, Walsh, and Zerwas[13], and for the JADE experimental data. The conclusion is again that the gluon jet is broader than the quark jet.

B. Λ, $\bar{\Lambda}$ yield - TASSO (Preliminary)

A natural question to ask is: are there more or less baryons in gluon jets compared with quark jets of the same energy? To investigate this problem, TASSO has studied the yield of Λ and $\bar{\Lambda}$ in the jets with jet energy around 7 GeV from three-jet events at W = 34 GeV, and compared the result with the corresponding yield from two-jet events at W = 14 GeV[35]. The three-jet analysis of Wu and Zobernig[36] was applied to the 20,014 hadronic events at W around 34 GeV, and 1402 events survived as three-jet candidates after the following cuts:

(a) $x_1 < 0.9$, where x_1 is defined in Sec. 4;

(b) for each of the three jets as determined by the three-jet analysis, the sum of the absolute values of the momenta of the charged particles is required to be larger than 1.5 GeV/c; and

(c) the angle between the normal to the events plane and the beam axis is required to be less than 70°.

The TASSO results on the yields of Λ and $\bar{\Lambda}$, after correction for acceptance, are tabulated in Table 4 for W = 14 GeV, 22 GeV, and around 34 GeV (separately for all events and for the three-jet candidates). Note that at 34 GeV the yield is significantly higher for the three-jet candidates than for all events:

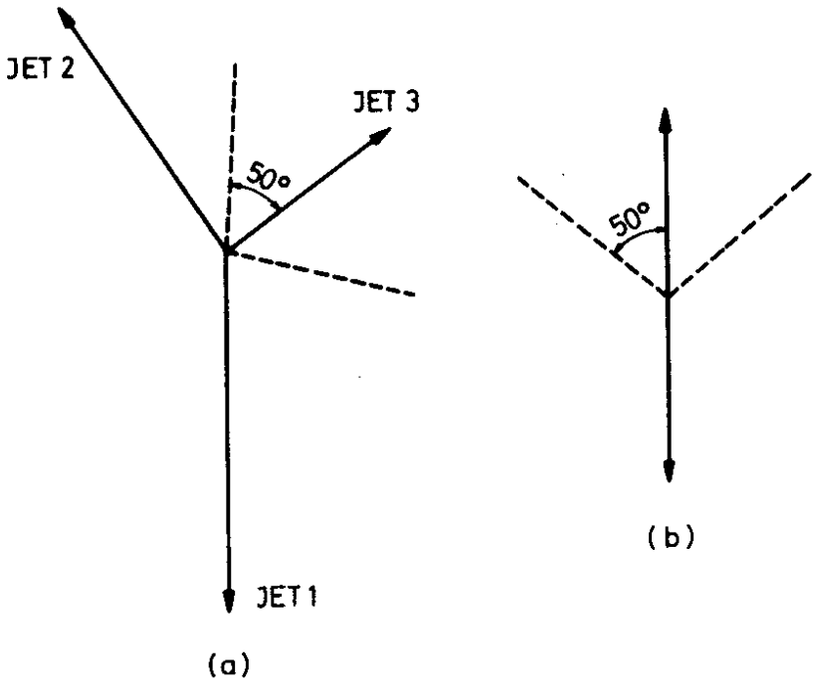

Fig. 24 - Kinematics for the JADE comparison of the p_T-distribution of (a) jet 3 (mostly gluon jet) at the center-of-mass energy of 33 GeV and of (b) two-jet events at 14 GeV. The p_T is calculated on the basis of the particles within a 50° cone of the jet axis.

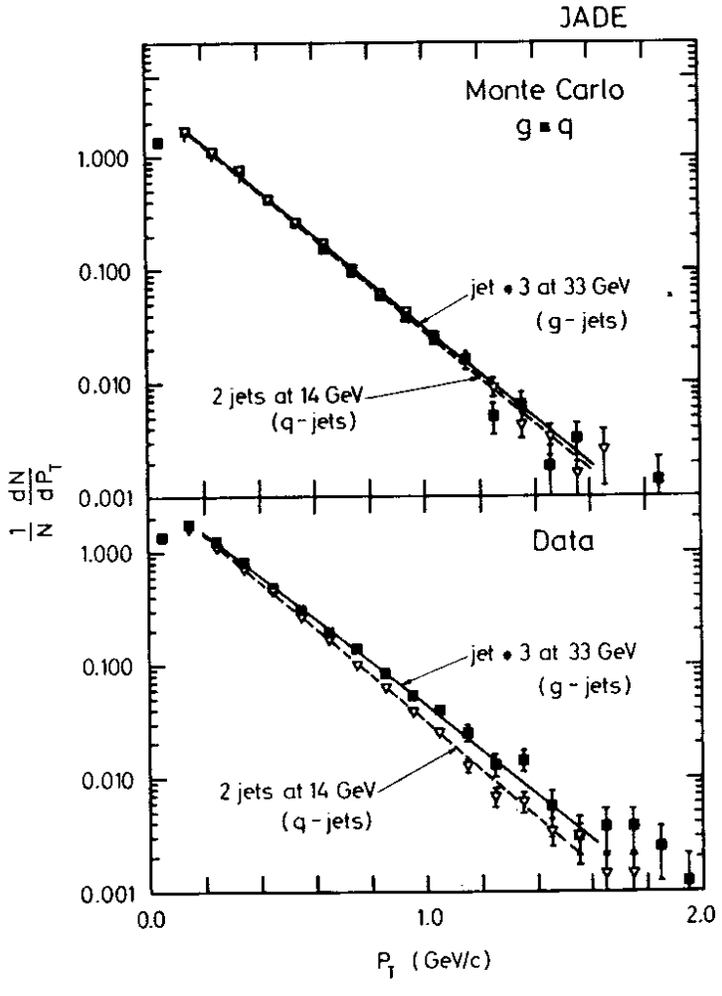

Fig. 25 - JADE comparison of the p_T-distribution of jet 3 (mostly gluon jet) at the center-of-mass energy of 33 GeV (upper straight lines) and of two-jet events at 14 GeV (lower straight lines). The upper figure is from the Monte Carlo of Hoyer et al., and the lower one from the experimental data.

$$\frac{\Lambda, \bar{\Lambda} \text{ yield for three-jet candidates}}{\Lambda, \bar{\Lambda} \text{ yield for all events}} = 2.0 \pm 0.5 ,$$

while the ratio of charged multiplicity is close to 1

$$\frac{\text{charged multiplicity for three-jet candidates}}{\text{charged multiplicity for all events}} = \frac{13.5}{11.8} .$$

Table 4 - Λ, $\bar{\Lambda}$ yield from TASSO data (preliminary).

W(GeV)	type of events	corrected Λ, $\bar{\Lambda}$ yield per event
34	all events	0.30 ± 0.04
34	3-jet events	0.59 ± 0.12
22	all events	0.22 ± 0.04
14	all events	0.13 ± 0.04

The jets from the three-jet candidates from W = 34 GeV are separated into three bins according to the jet energy: 4-9 GeV, 9-13 GeV, and >13 GeV. The Λ, $\bar{\Lambda}$ yields per jet for these three bins are shown in Fig. 26 together with those for all events at W = 14, 22, and 34 GeV

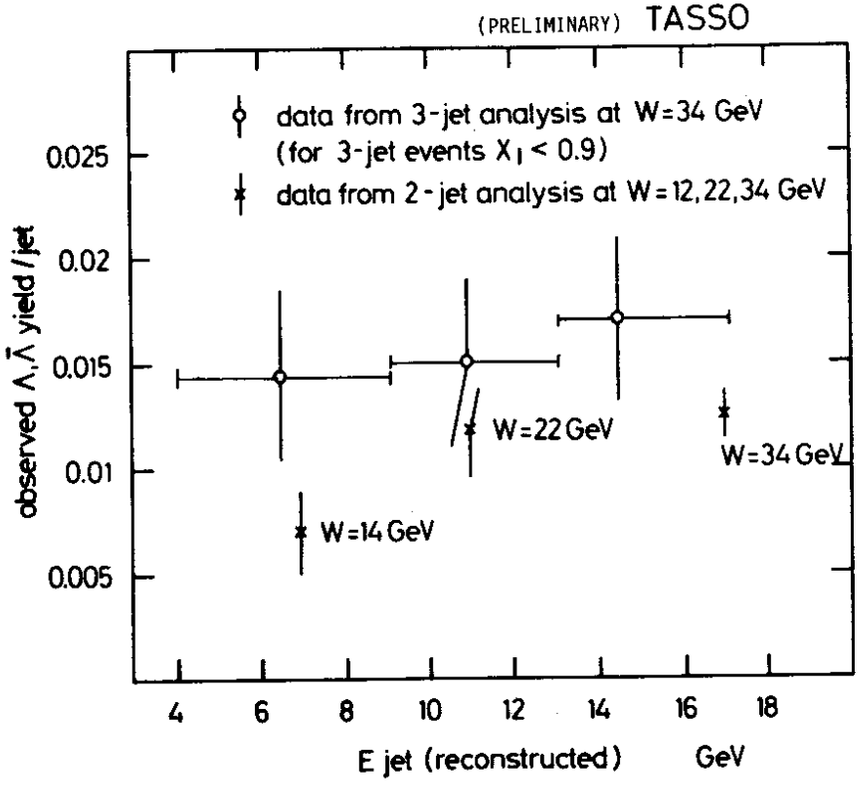

Fig. 26 - Observed Λ, $\bar{\Lambda}$ yields per jet from the three-jet candidates at W = 34 GeV, compared with those at W = 14, 22, and 34 GeV analyzed as two-jet events - TASSO.

analyzed as two-jet events. It is seen that the yield for the low energy jet, between 4 and 9 GeV, is higher than that for the 7 GeV jet from the two-jet events at W = 14 GeV. Since these low-energy jets at W = 34 GeV have about 50% gluon content, the results of FIG. 26 make it plausible that the yield of Λ and $\bar{\Lambda}$ is higher for gluon jet than for quark jet.

Related evidence has been obtained by the CLEO Collaboration at CESR[37]. They have found 0.25 ± 0.03 Λ, $\bar{\Lambda}$ per event at the resonance T(1S) but only 0.08 ± 0.01 at the nearby continuum. Since T (1S) decays predominantly into three gluons, this result is also interpreted to mean that there are more baryons in a gluon jet than in a quark jet.

6. PARTICLE IDENTIFICATION IN JETS

The knowledge of particle composition of the final state in e^+e^- annihilation is important for understanding of the fragmentation of quarks and gluons into hadrons. The following types of particles have been identified in jets and their inclusive cross sections measured:

$\pi^\pm$	:	TASSO, DELCO, JADE
π^0	:	TASSO, CELLO
$K^\pm$	:	TASSO, JADE
K_S	:	TASSO, PLUTO, JADE, MARK II
$p, \bar{p}$	:	TASSO, JADE, MARK II
Λ $\bar{\Lambda}$	:	JADE, TASSO, MARK II
ρ^0	:	TASSO
D*	:	MARK II, DELCO, TASSO (and CLEO at CESR)

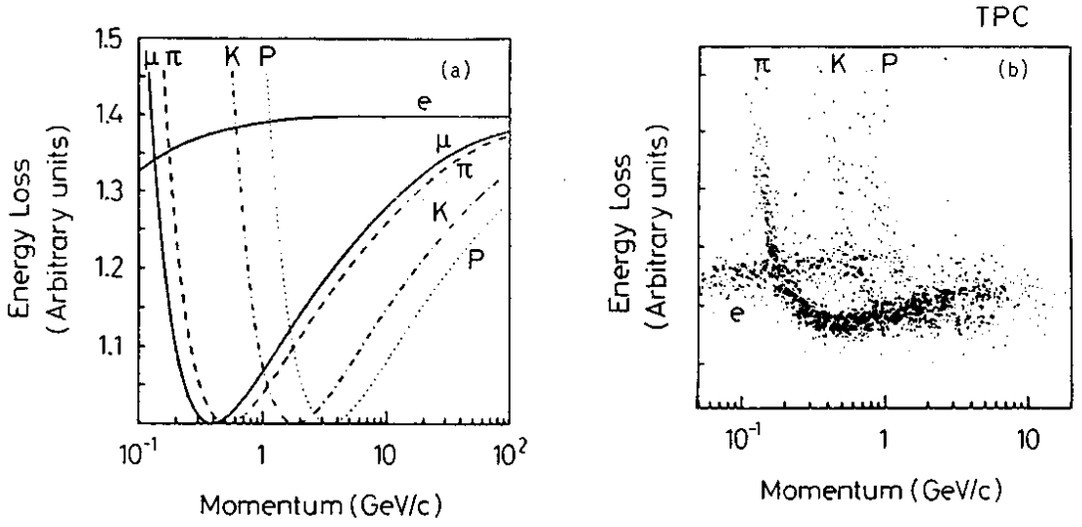

Fig. 27 - Particle separation by ionization loss in the relativistic rise region for the TPC detector at PEP: (a) the most probable energy loss vs. momentum, and (b) dE/dx vs. momentum for tracks in a sample of 1000 multihadron events at W = 29 GeV.

At PETRA and PEP, TASSO, DELCO and HRS are the only detectors equipped with Cerenkov counters. The momentum ranges where charged particle separation has been achieved at TASSO[38] are listed in Table 5. Recently, the separation of charged particles by dE/dx measurements has been accomplished at TPC[39] of PEP, and is shown in Fig. 27. In this section, we concentrate mostly on the recent results on inclusive particle spectra from TASSO.

Table 5 - Momentum ranges for $\pi^{\pm}/K^{\pm}/p,\bar{p}$ separation for the various systems in the TASSO detector.

	Momentum range in GeV/c for	
	$\pi^{\pm}/K^{\pm}$ separation	$K^{\pm}/p,\bar{p}$ separation
Inner time-of-flight system	0.3 - 1.0	0.4 - 1.4
Hadron arm time-of-flight system	0.5 - 1.5	1.0 - 2.0
Cerenkov counter system	above 0.8	3 - 6 and above 10
Combined	above 0.3	0.4 - 2.0, 3 - 6, and above 10

In Fig. 28 the differential cross sections $d\sigma/dp$ are given[26] for $\pi^{\pm}$, $K^{\pm}$, p, $\bar{p}$, Λ, and $\bar{\Lambda}$. The curves are drawn merely to guide the eye. As seen from this figure, the $\pi^{\pm}$ yield dominates for momenta below about 1 GeV/c. For example, the ratios $\pi^{\pm} : K^{\pm} : p, \bar{p}$ is approximately 100 : 10 : 1 at 0.5 GeV/c, but decrease to about 4 : 2 : 1 at 6 GeV/c. Because of phase space, all differential cross section $d\sigma/dp$ must approach zero as $p \to 0$, and hence must have maxima before dropping off. Furthermore, since the theoretically expected top quark has not yet been discovered experimentally, the total hadronic cross section is approximately proportional to s^{-1} from above the upsilon region to the highest PETRA energy. It is therefore useful to remove most of the phase-space effect and the energy dependence by considering the scaled cross sections

$$\frac{s}{\beta}\frac{d\sigma}{dx},$$

where $\beta = p/E$ is the velocity of the particle, and $x = E/E_{beam}$. The scaled inclusive cross sections for $(\pi^+ + \pi^-)$, $(K^+ + K^-)$, $(p + \bar{p})$, and $(\Lambda + \bar{\Lambda})$, as determined by TASSO, are shown in Fig. 29. Note that the cross section for $(K^+ + K^-)$, for example, is defined to be the sum of the cross section for K^+ and the cross section for K^-, not the cross section for the production of both a K^+ and a K^- in the same event. It is seen from Fig. 29 that the scaled cross sections for the various particles are rather similar in shape as functions of x.

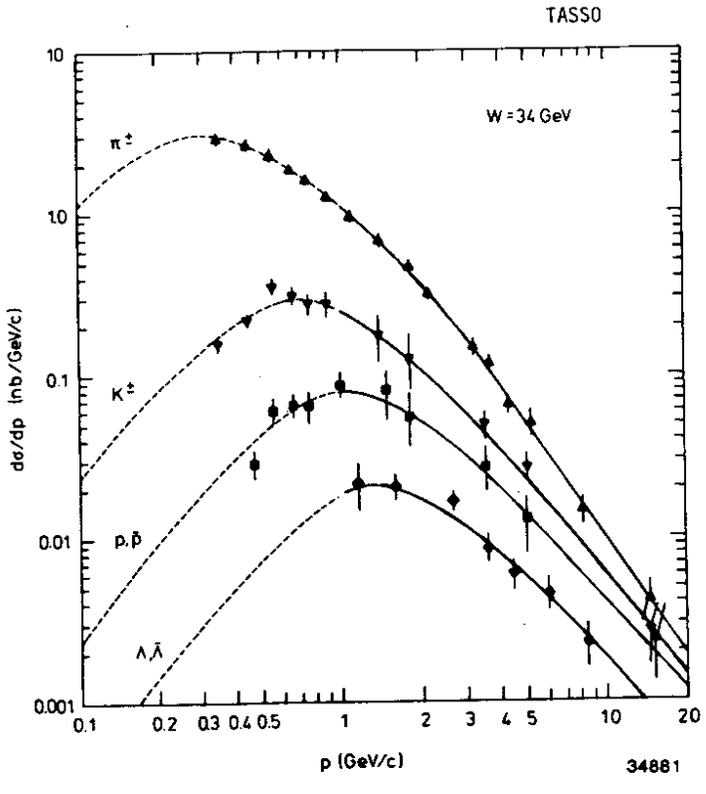

Fig. 28 - The differential cross sections for the inclusive production of $(\pi^+ + \pi^-)$, $(K^+ + K^-)$, $(p + \bar{p})$, and $(\Lambda + \bar{\Lambda})$ from TASSO at W = 34 GeV. The dashed curves are of the form $E/p^2\, d\sigma/dp \sim \exp(-bE)$ and the solid curves are drawn to guide the eye.

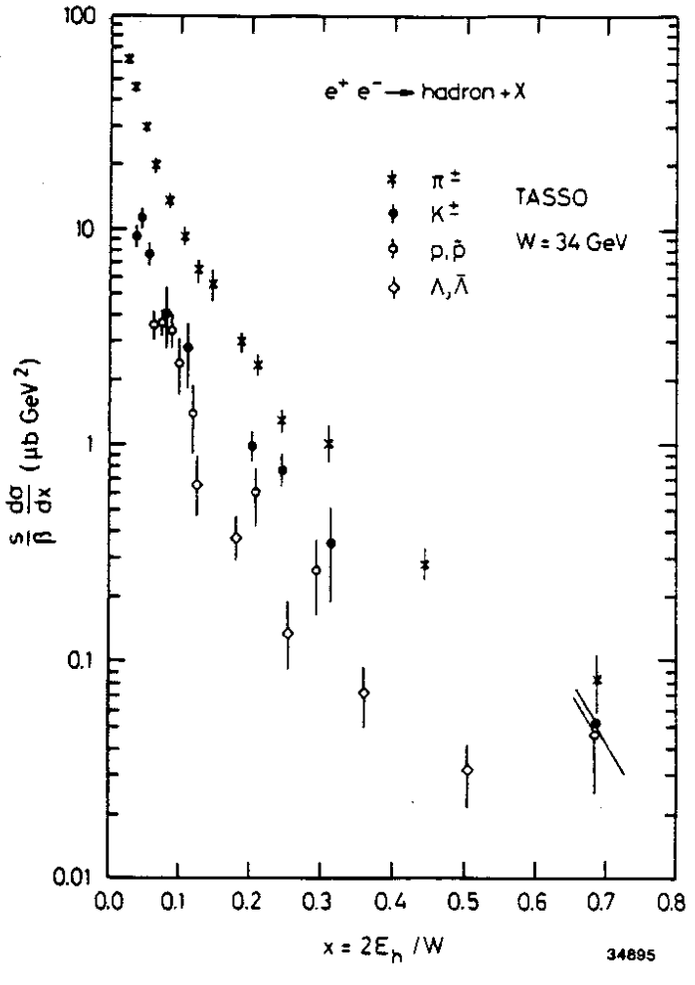

Fig. 29 - The TASSO scaled cross sections at 34 GeV for the inclusive production of $(\pi^+ + \pi^-)$, $(K^+ + K^-)$, $(p + \bar{p})$, and $(\Lambda + \bar{\Lambda})$.

The corresponding inclusive cross section for ρ^0 was recently obtained[22] at high energies and the result is shown in Fig. 30 (a) for center-of-mass energy 34 GeV. Comparison with Field-Feynman Monte Carlo leads to the following value for the fraction of producing pseudo-scalar mesons:

$$\frac{P}{P+V} = 0.42 \pm 0.08 \pm 0.15.$$

This value has already been used in connection with the α_s determination in second order discussed in Sec. 2D.

The average number of hadrons per event $\langle n_i \rangle$ is calculated according to

$$\langle n_i \rangle = \frac{\int_0^{p_{max}} \left(\frac{d\sigma}{dp}\right)_i dp}{\sigma_{tot}} , \qquad (7)$$

where σ_{tot} is the total hadronic cross section. The extrapolation of $(d\sigma/dp)_i$ to zero momentum, as well as the interpolation over the momentum intervals for which particles were not identified, was done by parametrizing the invariant cross sections in the form

$$(E_i/4\pi\, p_i^2)\,(d\sigma/dp)_i = \sum_m A_{im} \exp(-B_{im} E_i) \qquad (8)$$

The average particle multiplicities for hadronic events at 34 GeV are tabulated in Table 6. The majority of the $\pi^\pm$, $K^\pm$, ... presumably result from the decay of heavier mass particles. Thus about 35% of the protons and anti-protons come from the decays of Λ and $\bar{\Lambda}$. In the case of ρ^0, integration over the measure range of $0.1 < x < 0.7$ gives $0.41 \pm 0.04 \pm 0.08$ ρ^0 per event, and extrapolation to all x yields the value given in Table 6.

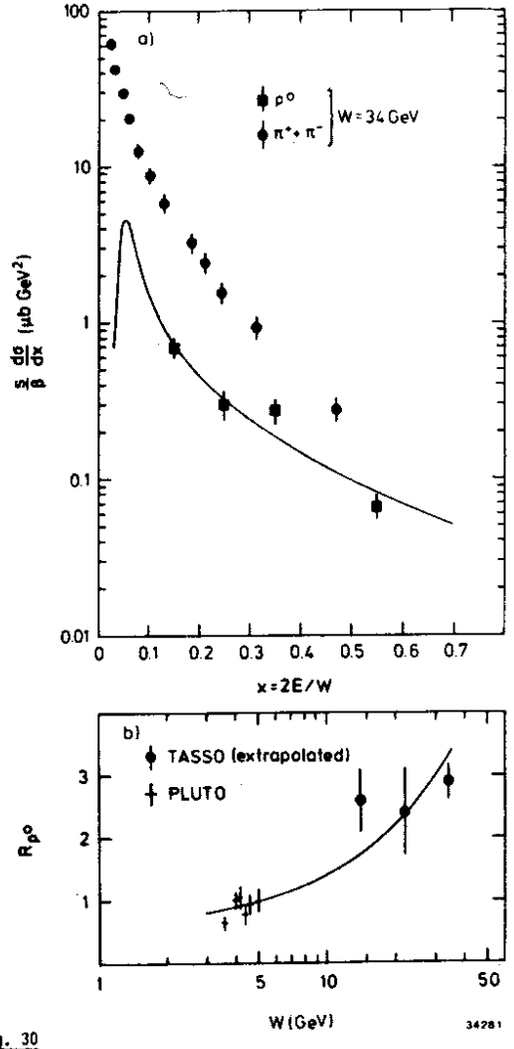

Fig. 30

TASSO data on the inclusive ρ^0 production. (a) The scaled cross section at the center-of-mass energy W = 34 GeV. Also shown is the cross section for $\pi^+ + \pi^-$ production at this energy. The smooth curve is the Field-Feynman Monte Carlo prediction for ρ^0 production assuming P/(P + V) =0.42. (b) $R_{\rho 0}$ for $e^+e^- \to \rho^0$ + hadrons as a function of W (errors shown are statistical only). The curve shows a fit to the TASSO charged particle multiplicity in e^+e^- → hadrons normalized to $R_{\rho 0}$.

Since $\rho^0 \to \pi^+ + \pi^-$, there are 0.73 π^+ and 0.73 π^- per event from ρ^0 decay alone. If the productions of ρ^+, ρ^0, and ρ^- are assumed to be equal, then the decay of ρ gives 1.46 π^+, 1.46 π^0, and 1.46 π^- per event. In other words, approximately 30% of the π's come from ρ decay.

Table 6 - The average number of various particles contained in a hadronic event at 34 GeV. The number of $\pi^\pm$ contains those from the decay of ρ^0, and that for $p + \bar{p}$ contain those from the decay of $\Lambda + \bar{\Lambda}$. The data are from TASSO.

Particle	$\langle n_i \rangle$
$\pi^\pm$	10.3 ± 0.4 [38]
π^0	6.1 ± 2.0 [40]
$K^\pm$	2.0 ± 0.2 [38]
$K^0 + \bar{K}^0$	1.6 ± 0.1 [41]
ρ^0	0.73 ± 0.06 [22]
$p + \bar{p}$	0.8 ± 0.1 [38]
$\Lambda + \bar{\Lambda}$	0.28 ± 0.04 [35]

The average particle multiplicities are compared with lower-energy data for ρ^0 in Fig. 30(b)[22], and for $\pi^\pm$, $K^\pm$, and $p,\bar{p}$ in Fig. 31[38]. In all cases, the increase is roughly proportional to that of the total multiplicity.

Another way to present the data is to show the particle fractions as functions of the hadron momentum. The recent TASSO data[38] are shown in Fig. 32. For low momenta, most of the particles are pions, as already discussed. At W = 34 GeV, the ratios $\pi^\pm$: $K^\pm$: $p,\bar{p}$ are 0.55 : 0.30 : 0.15 at 5 GeV/c, and are 0.45 : 0.30 : 0.25 above 10 GeV/c. The DELCO[42] and TPC[43] data, shown in Figs. 33 and 34 are consistent with those of TASSO.

7. SEARCH FOR CHARGED HIGGS AND TECHNIPIONS FROM 4-JET EVENTS - TASSO

In current theories of weak interactions, spin-zero particles are needed in order to generate masses for the intermediate vector bosons W and Z^0. In the original Higgs mechanism[4] used in the Weinberg-Salam theory[1], the spin-zero particle is elementary and has no charged partner. If there are charged partners, these charged Higgs[44] can be pair produced in e^+e^- annihilation and, similar to the neutral Higgs, decay predominantly into the heaviest quarks and leptons that are kinematically allowed. If, in contrast to the standard model, these spin-zero particles arise from dynamical symmetry breaking, then they are composite. While the concept of dynamical symmetry breaking is

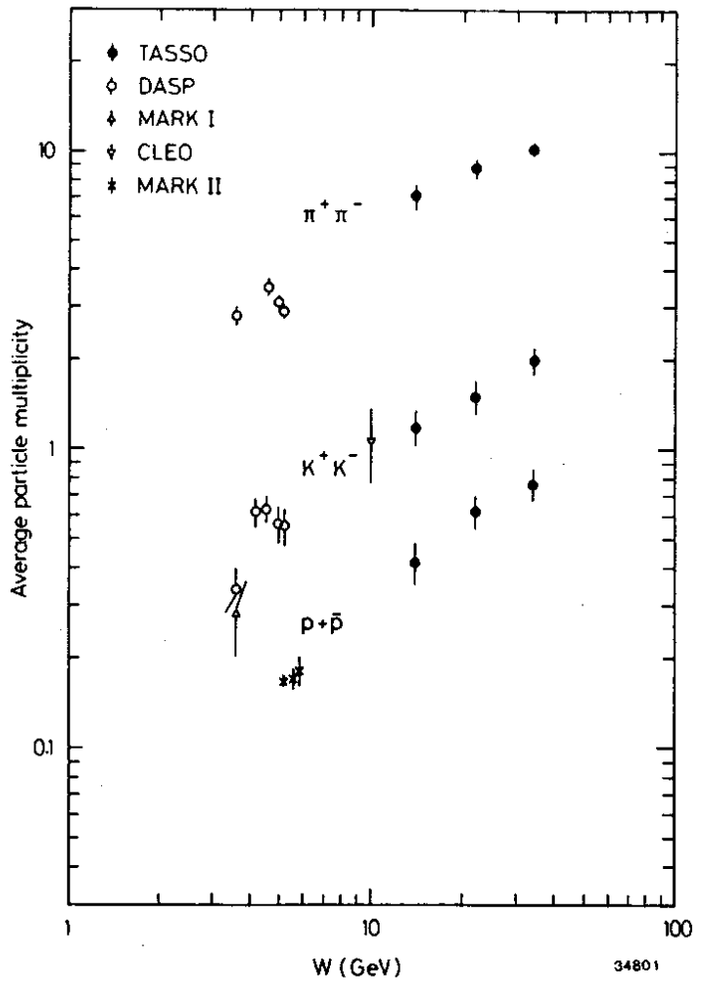

Fig. 31 - Average particle multiplicities for $\pi^\pm$, $K^\pm$, and $p,\bar{p}$ as functions of the center-of-mass energy W.

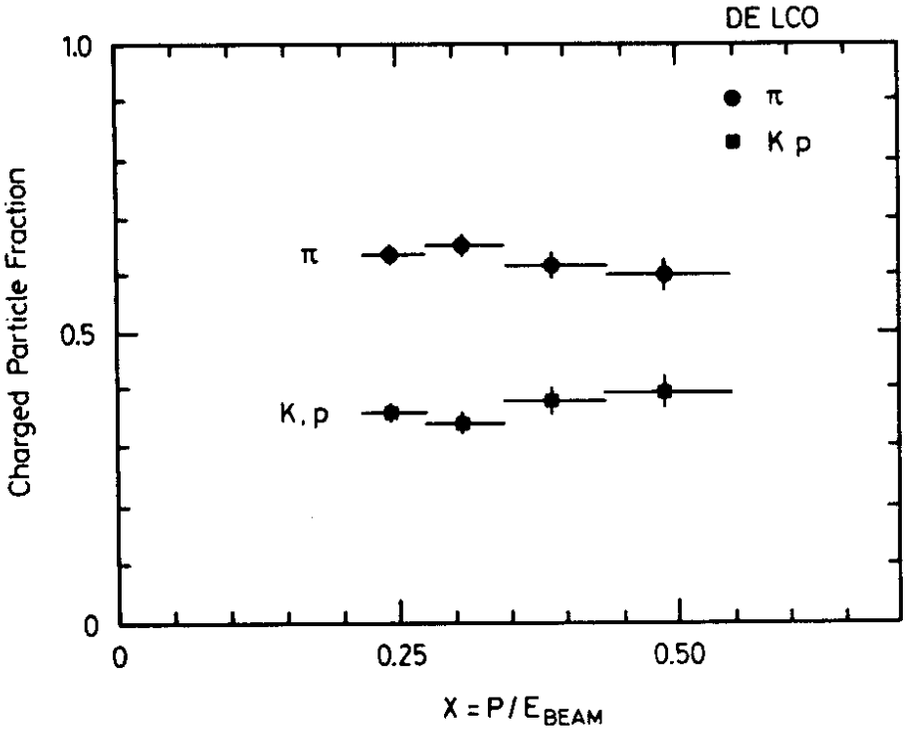

Fig. 33 - Fractions of $\pi^{\pm}$ and $K^{\pm}$ + $p,\bar{p}$ at W = 29 GeV from DELCO. The sum is of course equal to 1. The vertical error bars do not include an estimated systematic error of 0.1 on each point.

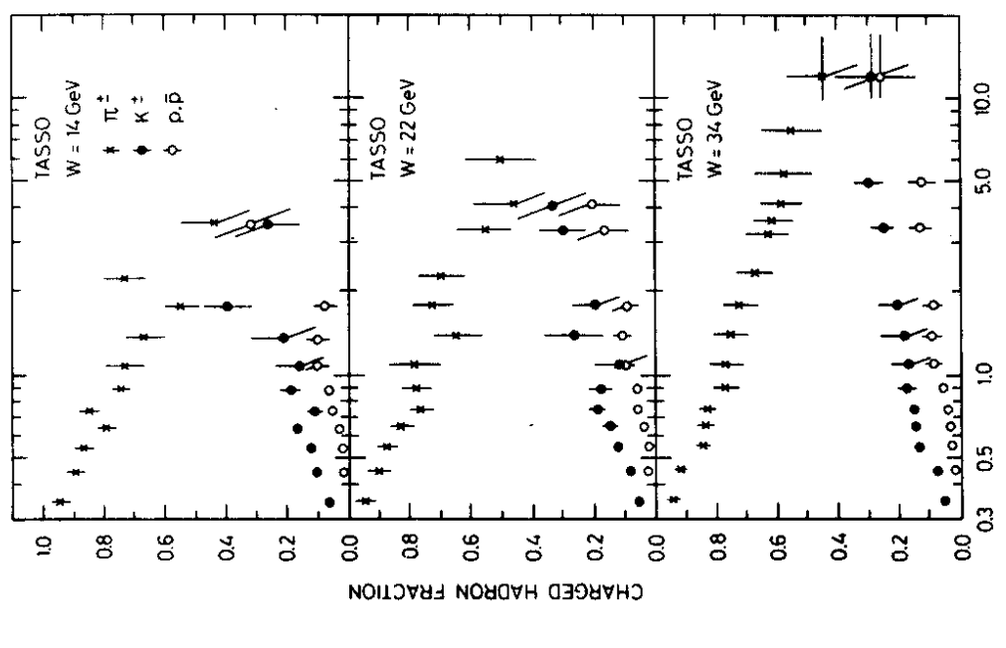

Fig. 32 Fractions of $\pi^{\pm}$, $K^{\pm}$, and $p,\bar{p}$ as functions of particle momentum at center-of-mass energy W = 14, 22, and 34 GeV. These data are from TASSO.

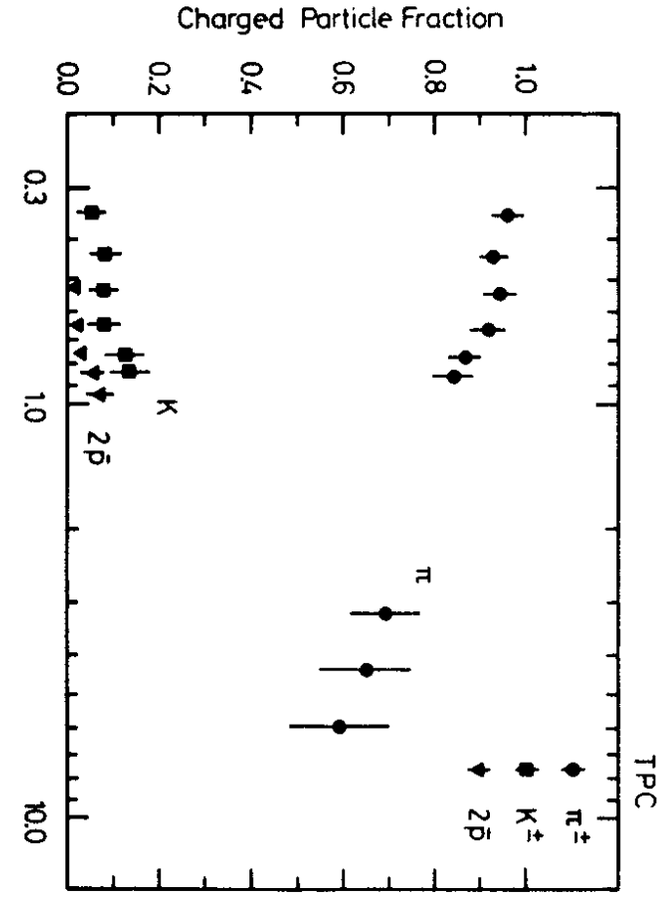

Fig. 34 - Fractions of $\pi^{\pm}$, $K^{\pm}$, and $2\bar{p}$ as functions of particle momentum at W = 29 GeV. These data are from TPC.

very attractive, specific additional assumptions are needed before concrete theoretical predictions can be obtained. At the present time, the most popular theory of this type is based on technicolor[45] and predicts the existence of spin-zero bosons of relatively low masses, called technipions. The mass of the charged technipions has been predicted to be in the range of 5 to 14 GeV[46]. Because of this low mass, this technicolor scheme, if correct, makes it possible to take a first look at the "mass problem" discussed in the Introduction. The decays into the heaviest kinematically allowed quarks and leptons are favored. The ratio of the leptonic and hadronic decay rates can be substantial or very small depending on the specific assumptions used[47]. If the leptonic decay mode is substantial, then the search for such spin-zero particles can be accomplished by studying the processes

$$e^+e^- \to H^+H^- \to (\tau\,\nu)\ (\text{hadrons}) \text{ and } (\tau^-\,\bar{\nu})\ (\tau^+\,\nu), \qquad (9)$$

where the symbol $H^{\pm}$ is used for both charged Higgs and technipions. In order to avoid any assumption about the size of the leptonic branching ratio, it is necessary to study also

$$e^+e^- \to H^+H^- \to \text{hadrons}. \qquad (10)$$

This process is shown schematically in Fig. 35, with the $H^{\pm}$ decaying into $c\bar{s}$ and $\bar{c}s$ before fragmentation into hadrons, giving rise to four jets.

The leptonic and semi-leptonic processes (9) have been studied by JADE[48], CELLO[49], MARK J[50], MARK II[51] and MAC[7]. The conclusion is that, with 95% confidence level, the hadronic branching ratio must be at least 80%.

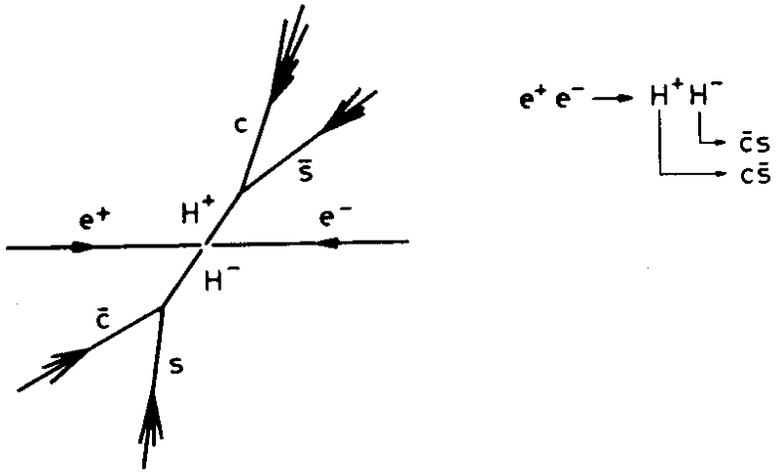

Fig. 35 - Schematic picture for the production and hadronic decay of $H^{\pm}$, leading to a four-jet final state.

With this knowledge, TASSO[52] undertook to study the process (10). The search for this process is not entirely straightforward since it has a small production cross section[53],

$$\frac{d\sigma}{d\Omega} = \frac{\alpha^2}{8s}\,\beta^3\,\sin^2\theta_H$$

and

$$R_{H^+H^-} = \frac{\sigma(e^+e^- \to H^+H^-)}{\sigma(e^+e^- \to \mu^+\mu^-)} = \frac{1}{4}\,\beta^3 \qquad (11)$$

where β is the velocity of $H^{\pm}$ in the c.m. system and θ_H is the production angle with respect to the beam axis.

The final state from the process (10) consists of four hadronic jets, as shown in Fig. 35. Therefore the fast four-jet analysis[54], involving the repeated application of the three-jet analysis[36] based on generalized sphericity, can be used. However, the jet masses cannot be neglected in this case because they may be comparable to the masses of $H^{\pm}$. This generalization of including the non-zero jet masses in the four-jet analysis is straightforward, if the true jet velocity is approximated by the observed jet velocity[52].

The four-jet analysis is applied to both the experimental data and the Monte Carlo event simulation. Two decay processes were studied:

Case (A) $e^+e^- \to H^+H^-$, $H^+ \to \bar{c}\,s$, $H^- \to c\,\bar{s}$

i.e. $H^{\pm}$ decay exclusively into $c\,\bar{s}$ quarks;

Case (B) $e^+e^- \to H^+H^-$, $H^+ \to \bar{c}\,s$ or $\bar{c}\,b$, $H^- \to c\,\bar{s}$ or $c\,\bar{b}$

with $H^{\pm}$ decaying equally into $c\,\bar{s}$ and $c\,\bar{b}$.

The data were subjected to a number of cuts in order to maximize the signal of $e^+e^- \to H^+H^-$ over the background contribution from QCD processes. First,good four-jet candidates are selected by applying cuts in the total visible energy of the event, the minimum observed jet energy, the minimum reconstructed jet energy, and the opening angle between the jets from the same $H^\pm$ decay. After these cuts, each event is described in terms of the three variables $\Delta E = E_1 + E_2 - E_{beam}$, $m_{av} = \frac{1}{2}(m_{12} + m_{34})$, and $\Theta_{av} = \frac{1}{2}(\Theta_{12} + \Theta_{34})$, where the various variables are shown in Fig. 36. Fig. 37 shows the two-dimensional plots in pairs of these three variables for Monte Carlo event with m_H = 10 GeV. It is seen that, roughly speaking, the events fill an ellipsoid whose size and orientation depends on m_H.

By a linear transformation on the three variables, the tilted ellipsoid is transformed into a sphere. The distributions of the experimental data and the Monte Carlo simulation are shown in Fig. 38 versus $(R/R_{rms})^3$, where R is the radius of the sphere and R_{rms} is the rms average of R over the Monte Carlo events for $e^+e^- \to H^+H^-$. It is seen that the two distributions are very different. In Fig. 39, the Monte Carlo distributions, one for $e^+e^- \to H^+H^-$ and the other for the QCD background, are compared with each other, and are found also to be quite different. The cut

$$R < R_{rms}$$

is therefore introduced to suppress the QCD background.

The analysis is repeated in steps of 100 MeV for m_H between 5 GeV and 14.5 GeV. With the cuts described above, the experimental data are compared with the Monte Carlo expectation in Fig. 40. The surviving

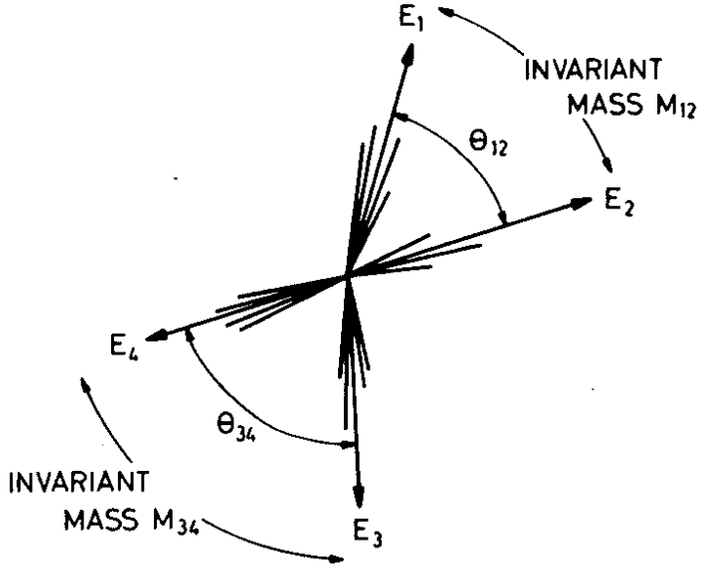

Fig. 36 - Some of the kinematic variables for a four-jet event from the pair production of $H^\pm$. The jets 1 and 2 are from the decay of one H, and jets 3 and 4 are from the other H.

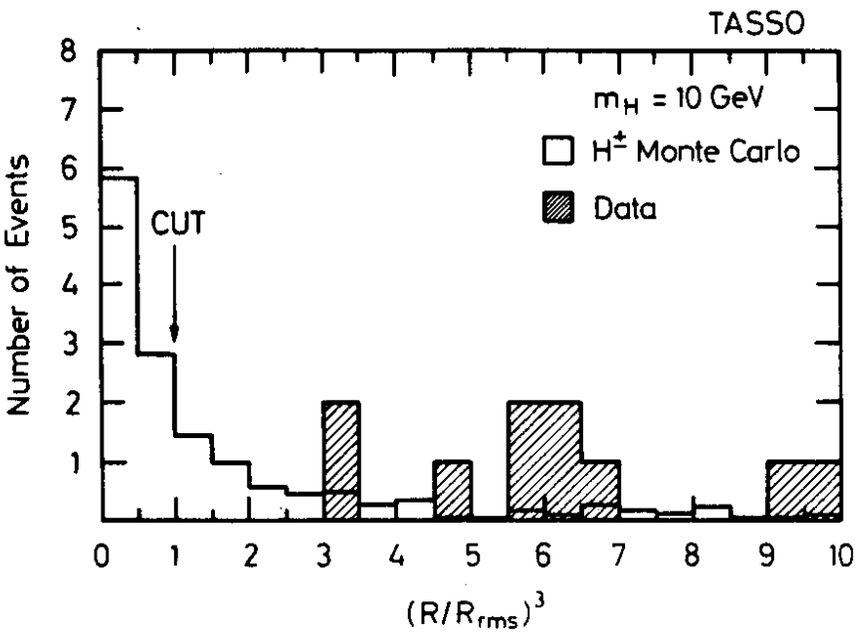

Fig. 38 - Monte Carlo and data (shaded) distributions of the one-dimensional variable $(R/R_{rms})^3$ analyzed at m_H = 10 GeV. The Monte Carlo distribution is normalized to the same total luminosity as the data. The position of cut $R = R_{rms}$ is indicated.

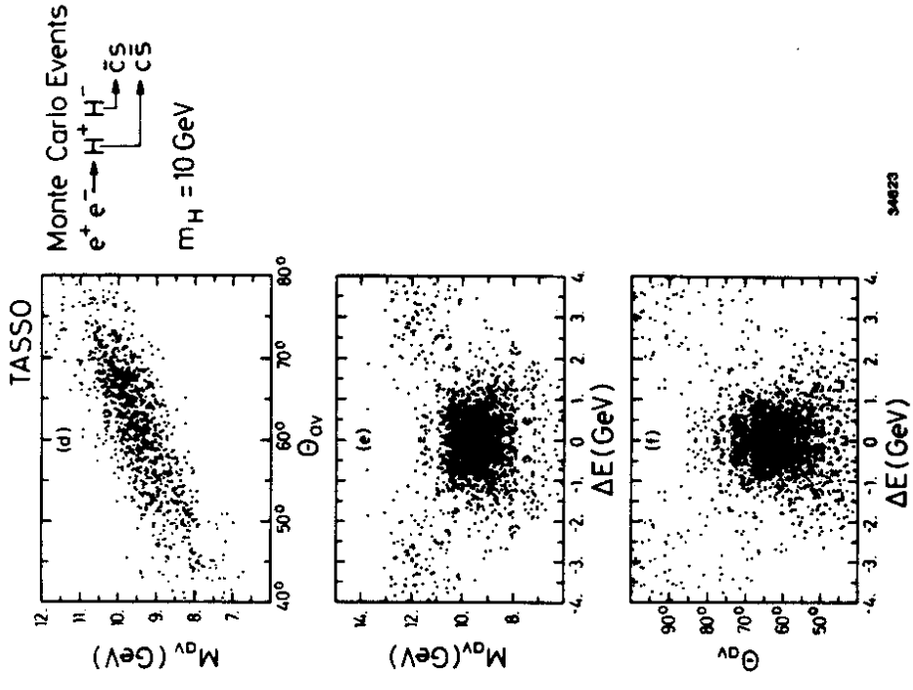

Fig. 37
Two-dimensional Monte Carlo event distributions of pairs of the three variables, the average reconstructed mass m_{av}, the average reconstructed opening angle θ_{av}, and the difference ΔE between the beam energy and the sum of the reconstructed energies of jet 1 and jet 2.

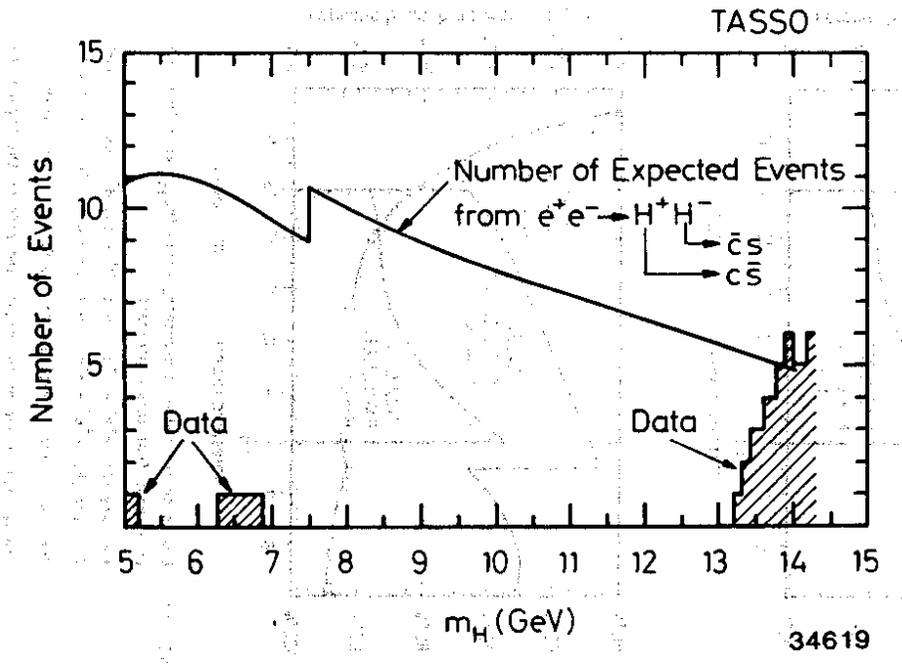

Fig. 40 - Number of expected events after all the cuts as a function of m_H for $e^+e^- \to H^+H^-$ with $H^+ \to c\bar{s}$, $H^- \to \bar{c}s$. Also shown is the number of events observed by TASSO as a function of m_H.

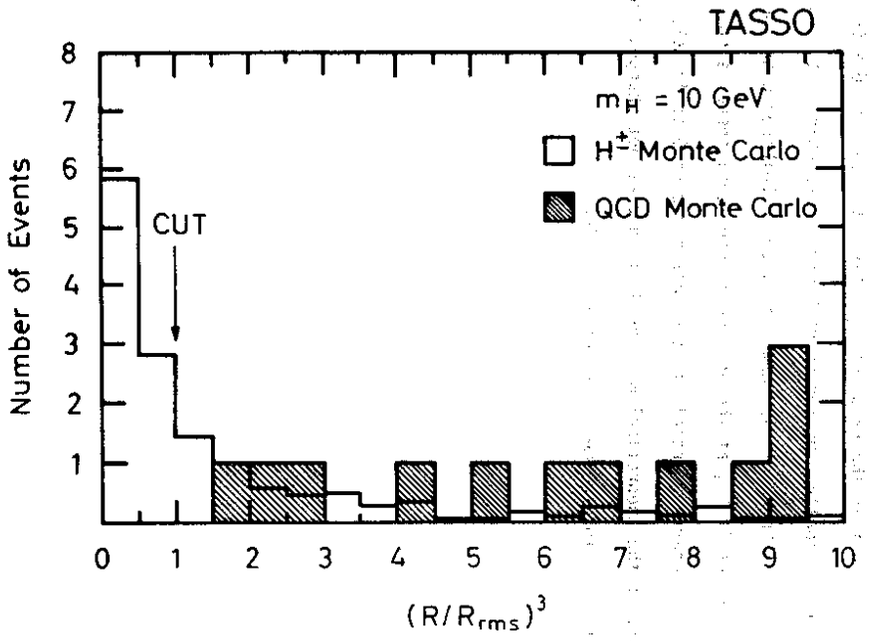

Fig. 39 - Comparison, at m_H = 10 GeV, of the $H^\pm$ and QCD Monte Carlo distributions of the one-dimensional variable $(R/R_{rms})^3$. The cut at $R = R_{rms}$ is also shown.

events above 13 GeV are consistent with QCD expectation. Note that Fig. 40 is really a compilation of many similar but independent analyses, each corresponding to a different value of m_H. In particular, the surviving event in the range of m_H between 6.3 GeV and 6.9 GeV is the same event. Finally, the region of hadronic branching ratio excluded by this TASSO result is shown in Fig. 41. Combined with the previous JADE result[48], at the 95% confidence level there is no point-like spin-zero charged particle in the mass range of 5 to 13 GeV. In particular, if the theoretical mass prediction does not change, the standard technicolor scheme is essentially ruled out.

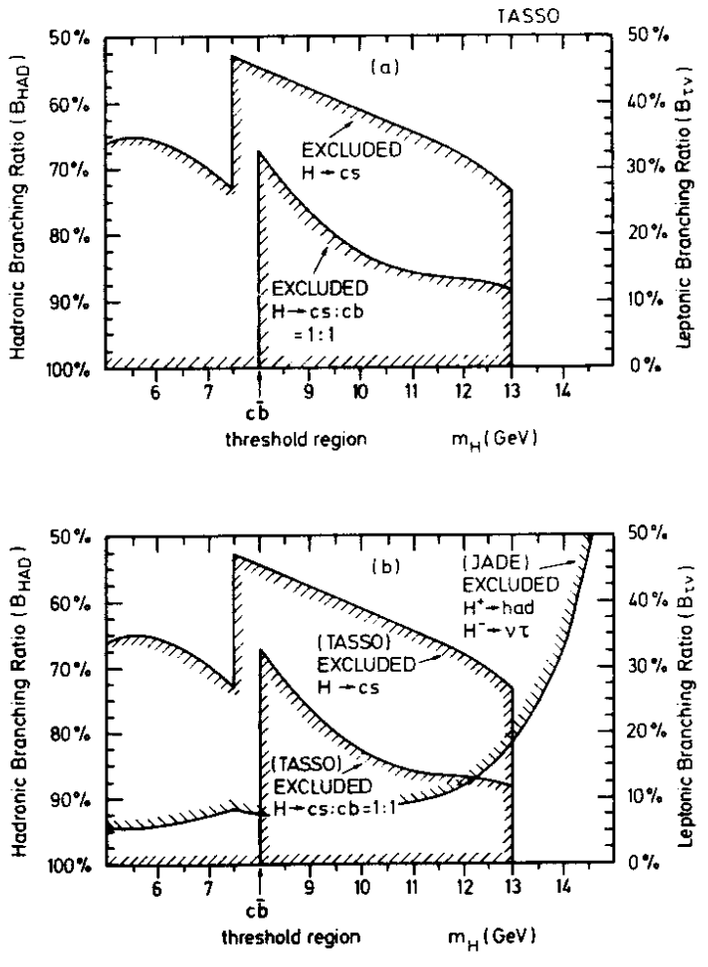

Fig. 41 -(a) : Limits on the hadronic branching ratio (B_{had}) as a function of $H^{\pm}$ mass from this experiment

for case (A) $e^+e^- \to H^+H^-$ with $H^+ \to c\bar{s}$, $H^- \to \bar{c}s$ and
for case (B) $e^+e^- \to H^+H^-$ with $(H \to cs) : (H \to cb) = 1 : 1$

The shaded area is excluded at the 95% confidence level.

The vertical scale on the right hand side of the figure indicates the corresponding leptonic branching ratio ($B_{\tau\nu}$) if the sum of $B_{had} + B_{\tau\nu} = 1$.

(b) : Limits on the leptonic branching ratio from JADE for $H^+ \to \tau^+\nu$, $H^- \to \tau^-\bar{\nu}$ or $H^+ \to \tau^+\nu$, $H^- \to$ hadrons superimposed on Fig. 41 (a).

Acknowledgements

I wish to thank Professors G.Feldman, F.Gilman and D.W.G.S.Leith for their hospitality at the 1982 SLAC Summer Institute on Particle Physics. I also wish to thank the many colleagues who provided me with their data. I am grateful to P.J.Dornan, A.Petersen, G.Rudolph, J. Sedgbeer, P.Söding, B.H.Wiik and G.Wolf for helpful and stimulating discussions.

REFERENCES

1) S.L. Glashow, Nucl. Phys. 22, 579 (1961)
S.Weinberg, Phys.Rev.Lett. 19, 1264 (1967)
A.Salam, Proceedings of the Eighth Nobel Symposium, May 1968, ed.: N.Svartholm (Wiley, 1968), p.367

2) B.H. Wiik, Proc. Intern. Neutrino Conf. (Bergen, Norway, 1979) p. 113
P.Söding, Proc. EPS Intern. Conf. on High energy physics (Geneva, Switzerland, 1979) p. 271
TASSO Collab., R.Brandelik et al., Phys. Lett. 86B (1979) 243
MARK-J Collab., D.P. Barber et al., Phys.Rev.Lett. 43 (1979) 830
PLUTO Collab., Ch.Berger et al., Phys.Lett. 86B (1979) 418
JADE Collab., W.Bartel et al., Phys.Lett. 91B (1980) 142

3) JADE Collaboration, W.Bartel et al., Phys.Lett. 108B (1982) 140
CELLO Collaboration, H.J.Behrend et al., DESY 82-019 (1982)
TASSO Collaboration, R.Brandelik et al., Phys.Lett. 110B (1982) 173
MARK J Collaboration, B.Adeva et al., Phys.Rev.Lett. 48 (1982) 1701
M.Davier, Rapporteur's talk, Proceedings of the 21st International Conference on High Energy Physics, Paris, 26-31 July 1982 and LAL (Orsay) Report 82/39 October 1982

4) P.W.Higgs, Phys.Rev.Lett. 12 (1964) 132; 13 (1964) 508
P.W.Higgs, Phys.Rev. 145 (1966) 1156
F.Englert, and R. Brout, Phys.Rev.Lett. 13 (1964) 321
G.S.Guralnik, C.R.Hagen, and T.W.B.Kibble, Phys.Rev.Lett. 13 (1964) 585
T.W.B.Kibble, Phys.Rev. 155 (1967) 1554

5) CELLO Collaboration, H.J.Behrend et al., DESY 82-061 (1982)

6) JADE Collaboration, W.Bartel et al., DESY 82-060 (1982)

7) MAC Collaboration (presented by D.Ritson), Proceedings of the21st International Conference on High Energy Physics, Paris, 26-31 July 1982

8) MARK II Collaboration, D.Schlatter et al., Phys.Rev.Lett. 49 (1982) 521

9) MARK J Collaboration (presented by J.Burger), Proceedings of the 21st International Conference on High Energy Physics, Paris, 26-31 July 1982

10) PLUTO Collaboration, Ch.Berger et al., Phys.Lett. 97B (1980) 459

11) TASSO Collaboration, R.Brandelik et al., Phys.Lett. 94B (1980) 437 and to be published

12) C.Basham, L.Brown, S.Ellis, and S.Love, Phys.Rev. D 19, (1979) 2018, and 24, (1981) 2383

13) P.Hoyer, P.Osland, H.E.Sander, T.F.Walsh and P.M.Zerwas, Nucl.Phys. B161, (1979) 349
A.Ali, E.Pietarinen, G.Kramer and J.Willrodt, Phys.Lett. 93B, (1980) 155

14) B.Andersson, G.Gustafson, and T.Sjöstrand, Z.Phys. C6 (1980) 235
T.Sjöstrand, Lund Preprint, LU TP 80-3(1980), LU TP 82-3(1982)
B.Andersson, G.Gustafson, and T.Sjöstrand, Nucl.Phys. B197 (1982) 45

15) MARK II Collaboration (presented by R.J.Hollebeek), Proceedings of 1981 International Symposium on Lepton and Photon Interactions at High Energies, Bonn, August 24-29, 1981

16) J.Ellis, M.K.Gaillard and G.G.Ross, Nucl.Phys. B111 (1976) 253
T.A.DeGrand, Y.J.Ng and S.-H.Tye, Phys.Rev. D16 (1977) 3251

17) R.D.Field and R.P.Feynman, Nucl.Phys. B136 (1978) 1

18) R.K.Ellis, D.A.Ross, A.E.Terrano, Phys.Lett. 45 (1980) 1226

19) K.Fabricius, G.Kramer, G.Schierholz, I.Schmitt, Z. Phys. C11 (1982) 315;

A.Ali, J.G.Körner, G.Kramer, Z.Kunszt, E.Pietarinen, G.Schierholz, and J.Willrodt, Phys.Lett. 82B (1979) 285, and Nucl.Phys. B167 (1980) 454

20) K.J.F.Gaemers and J.A.M.Vermaseren, Z.Physik C7 (1980) 81

21) T.Gottschalk, Phys.Lett. 109B (1982) 331, showed that the results of Fabricius et al. are consistent with those of R.K.Ellis et al. in the limit where the two different definitions of "thrust" are identical. See also G.Kramer, DESY 82-029 (1982)

22) TASSO Collaboration, R.Brandelik et al., DESY 82-046 (1982)

23) TASSO Collaboration, R.Brandelik et al., Phys.Lett. 113B (1982) 499

24) JADE Collaboration (presented by G.Heinzelmann), Proceedings of the 21st International Conference on High Energy Physics, Paris, 26-31 July, 1982

25) MARK II Collaboration (presented by G.Trilling), Proceedings of the 21st International Conference on High Energy Physics, Paris, 26-31 July, 1982

26) G.Wolf, Rapporteur's talk, Proceedings of the 21st International Conference on High Energy Physics, Paris, 26-31 July, 1982

27) TASSO Collaboration, R.Brandelik et al., Phys.Lett. 94B (1980) 437

28) PLUTO Collaboration, Ch.Berger et al., Phys.Lett. 97B (1980) 459

29) CELLO Collaboration, H.J.Behrend et al., Phys.Lett. 110B (1982) 329

30) TASSO Collaboration (presented by D.Lüke), Proceedings of the 21st International Conference on High Energy Physics, Paris, 26-31 July, 1982

31) Sau Lan Wu, Rapporteur talk, Proceedings of the 1981 SLAC Summer Institute on Particle Physics, July 27 - August 7, 1981, SLAC, Stanford, California, USA

32) J.Ellis and I.Karliner, Nucl.Phys. B148 (1979) 141

33) JADE Collaboration, W.Bartel et al., DESY 82-086 (1982)

34) JADE Collaboration, to be published

35) TASSO Collaboration, R.Brandelik et al., Phys.Lett. 105B (1981) 75 and to be published

36) Sau Lan Wu and Georg Zobernig, Z.Phys. C - Particles and Fields 2, (1979) 107

37) CLEO Collaboration (presented by F.M.Pipkin) Proceedings of the 21st International Conference on High Energy Physics, Paris, 26-31 July, 1982

38) TASSO Collaboration, M.Althoff et al., DESY 82-070 (1982)

39) TPC Collaboration (presented by B.Cabioud at IEEE Meeting, Washington, D.C., October 1982), TPC-LBL-82-76

40) TASSO Collaboration, R.Brandelik et al., Phys.Lett. 108B (1982) 71

41) TASSO Collaboration, R.Brandelik et al., Phys.Lett. 94B (1980) 91 and to be published

42) DELCO Collaboration (presented by J.Kirkby),Proceedings of the 21st International Conference on High Energy Physics, Paris, 26-31 July, 1982

43) TPC Collaboration, to be published

44) E.Golowich and T.C.Yang, Phys.Lett. 80B, 245 (1979)
L.N.Chang and J.E.Kim, Phys.Lett. 81B, 233 (1979)
H.E.Haber, G.L.Kane and T.Sterling, Nucl.Phys. B161, 493 (1979)
G.Barbiellini et al., DESY 79-027 (1979), and references therein

45) S.Weinberg, Phys.Rev. D13, 974 (1976); D19, 1277 (1979)
L.Susskind, Phys.Rev. D20, 2619 (1979)
S.Dimopoulos and L.Susskind, Nucl.Phys. B155, 237 (1979)
E.Eichten and K.D.Lane, Phys.Lett. 90B, 125 (1980)
M.A.B.Beg, H.D.Politzer and P.Ramond, Phys.Rev.Lett. 43, 1701 (1979)
S.Dimopoulos, Nucl.Phys. B168, 69 (1980)
M.E.Peskin, Nucl.Phys. B175, 197 (1980)
S.Dimopoulos, S.Raby and P.Sikivie, Nucl.Phys. B176, 449 (1980)
S.Dimopoulos, S.Raby and G.L.Kane, Nucl.Phys. B182, 77 (1981)
E.Fahri and L. Susskind, Phys.Rep. 74, 277 (1981)
A.Ali, DESY 81-032 (1981)
G.Barbiellini et al., DESY 81-064, and references therein

46) S.Dimopoulos, Nucl.Phys. B168, 69 (1980)
M.E.Peskin, Nucl.Phys. B175, 197 (1980)
J.Preskill, Nucl.Phys. B177, 21 (1981)
S.Chadha and M.E.Peskin, Nucl.Phys. B185, 61(1981) and B187, 541(1981)

47) J.Ellis, M.K.Gaillard, D.V.Nanopoulos and P.Sikivie, Nucl.Phys. B182, 529 (1981)

48) JADE Collaboration, W.Bartel et al., Phys.Lett. 114B, 211(1982)

49) CELLO Collaboration, H.J.Behrend et al., DESY 82-021 (1982)

50) MARK J Collaboration, A.Adeva et al., LNS Technical Report Number 125 (1982)

51) MARK II Collaboration, C.A.Blocker et al.,SLAC-PUB-2923 (1982)

52) TASSO Collaboration, M.Althoff et al., DESY 82-069 (1982)

53) N.Cabibbo and R.Gatto, Phys.Rev. 124, 1577 (1961)

54) Sau Lan Wu, Z.Phys. C - Particles and Fields 9, 329 (1981)